universität wien

MASTERARBEIT / MASTER'S THESIS

Titel der Masterarbeit / Title of the Master's Thesis

„Establishment of [^{18}F]4-fluoroglutamine"

verfasst von / submitted by

Miriam Schobesberger, BSc

angestrebter akademischer Grad / in partial fulfilment of the requirements for the degree of

Master of Science (MSc)

Wien, 2023 / Vienna 2023

Studienkennzahl lt. Studienblatt / degree programme code as it appears on the student record sheet:	UA 066 862
Studienrichtung lt. Studienblatt / degree programme as it appears on the student record sheet:	Masterstudium Chemie
Betreut von / Supervisor:	Assoz. Prof. Dr. Thomas Mindt, Privatdoz.
Mitbetreut von / Co-Supervisor:	Dr. rer. nat. Chrysoula Vraka, MSc

Acknowledgements

First and foremost, I would like to thank my supervisor Dr. rer. nat. Chrysoula Vraka, MSc for her guidance throughout the whole process and for sharing her vast knowledge and experience in this field of research with me. I am impressed by her work ethos and appreciate her patience and positivity. My gratitude also goes to Prof. Dr. Thomas L. Mindt for his trust and accepting to supervise this thesis, an opportunity I highly appreciate.

Furthermore, I would like to thank Maximilian Krisch, MSc for his kindness and support, especially during the establishment of the synthesis on the module. Many thanks also go to Ap. Prof. Mag. Dr. Cécile Philippe for sharing her expertise and technical experience concerning radiosynthesis, Ing. Dr. Marius Ozenil, MSc for his advice during the establishment of the synthesis method, Ing. Thomas Zenz for his technical support and Mag. pharm. Eva-Maria Patronas for providing us with cells for our in vitro studies. I would further like to express my gratitude towards the entire Division of Nuclear Medicine in the general hospital of Vienna for being welcoming and open to help in my moments of doubt.

Lastly, I would like to thank my parents in particular, and the rest of my family for their moral support and kindness, as well as my friends, who each in their own way always found ways to lift me up throughout the process.

Abstract

The amino acid glutamine is, besides glucose, a major nutrient for tumour cells, supplying energy and building blocks for the endogenous synthesis of biomolecules. Apart from the Warburg effect, which characterises the metabolism of the majority of tumours and refers to aerobic glycolysis despite the presence of oxygen, tumour cells can also be reprogrammed to be “glutamine addicted”. This describes a higher dependency on glutamine compared to non-malignant cells due to upregulation of various steps in the metabolic pathway. This may be an indication for using a radiolabelled glutamine analogion as an alternative to the gold standard in positron emission tomography (PET), which is 2-[^{18}F]-fluoro-2-deoxy-D-glucose (2-[^{18}F]FDG). 2-[^{18}F]FDG faces some limitations including non-specific uptake in immune cells, which is why this tracer is also applied for imaging of inflammation and infection. The aim of this thesis was to establish an automated production method of (2S,4R)-[^{18}F]4-fluoroglutamine ([^{18}F]4-FGln) on an ELIXYS FLEX/CHEM automated synthesizer based on two previously reported methods. This included the development of purification and quality control methods. Subsequently, the goal was to conduct in vitro [^{18}F]4-FGln uptake studies in tumour cells and comparison with the uptake of 2-[^{18}F]FDG and tritium-labelled glutamine.

Zusammenfassung

Die Aminosäure Glutamin ist neben Glukose ein Hauptenergielieferant für Tumorzellen und stellt eine Kohlenstoff- und Stickstoffquelle für die endogene Biosynthese diverser Moleküle dar. Der sogenannte Warburg Effekt beschreibt eine Veränderung des Glukosestoffwechsels, welche in den meisten Tumorarten auftritt, aufgrund derer aerobe Glykolyse selbst unter sauerstoffreichen Bedingungen bevorzugt wird. Tumorzellen können jedoch auch genetische Veränderungen in Richtung einer erhöhten Abhängigkeit von Glutamin erfahren, welche durch Hochregulierung diverser Schritte im Stoffwechsel von Glutamin zustande kommt. Dies könnte eine Indikation für die Entwicklung eines radioaktiv markierten Glutamin-analogons sein, welches als Alternative für die in der Positronen-Emissions-Tomographie (PET) weit verbreitete 2-[^{18}F]-fluoro-2-deoxy-D-glucose (2-[^{18}F]FDG) dienen könnte. Trotz großen Erfolgs hat 2-[^{18}F]FDG diverse Limitationen, wie zum Beispiel die unspezifische Aufnahme in Immunzellen. Deshalb wird dieser PET-tracer auch zur Bildgebung von Entzündungsgeschehen und Infektionen verwendet. Ziel dieser Masterarbeit war es somit, eine automatisierte Produktionsmethode von (2S,4R)-[^{18}F]4-fluoroglutamine ([^{18}F]4-FGln) auf einem ELIXYS FLEX/CHEM Synthesemodul aufzusetzen, basierend auf zwei publizierten Methoden. Dies inkludierte die Etablierung von Methoden zur Aufreinigung und Qualitätskontrolle. Daraufhin sollte die in vitro Aufnahme von [^{18}F]4-FGln in Tumorzellen mit der von 2-[^{18}F]FDG und Tritium-markiertem Glutamin verglichen werden.

Table of contents

List of tables

Table of figures

List of abbreviations

5' adenosine monophosphate-activated protein kinase	AMPK
(2S,4S)-tert-butyl-2-(tert-butoxy-carbonylamino)-5-oxo-4-(tosyloxy)-5-(2,4,6-trimethoxybenzylamino)-pentanoate)	tosylate - precursor
(2S,4R)-[^{18}F]4-fluoroglutamate	[^{18}F]4-FGlu
(2S,4R)-[^{18}F]4-fluoroglutamine	[^{18}F]4-FGln
[^{18}F]fluoroethyltyrosine	[^{18}F]FET
[^{18}F]fluorothymidine	[^{18}F]FLT
[^{18}F]sodium fluoride	[^{18}F]NaF
14-(R,S)-[^{18}F]-fluoro-6-thiaheptadecanoic acid	[^{18}F]FTHA
2-[^{18}F]-fluoro-2-deoxy-D-glucose	2-[^{18}F]FDG
2-deoxy-D-glucose	2-DG
2,4,6-trimethoxybenzyl	Tmob
6-[^{18}F]fluoro-L-3,4-dihydroxyphenylalanine	[^{18}F]FDOPA
acetonitrile	ACN
adenosine triphosphate	ATP
alpha-ketoglutarate	α-KG
amidohydrolases	GLS, GLS2
asparagine	Asn
bi-molecular nucleophilic substitution	S_N2
brown adipose tissue	BAT
coefficient of variation	CV
computed tomography	CT
cysteine	Cys
foetal bovine serum	FBS
flavin adenine dinucleotide (fully reduced)	$FADH_2$
glucose transporter	GLUT
glutamate dehydrogenase	GLUD
glutaminase	GLS1
glutathione	GSH
guanosine triphosphate	GTP
high performance liquid chromatography	HPLC
hypoxia-inducible factor	HIF

Kirsten rat sarcoma viral oncogene	KRAS
large amino acid transporter 1	LAT1
linear energy transfer	LET
magnetic resonance spectroscopy (imaging)	MRS(I)
mammalian target of rapamycin complex 1	mTORC1
methanol	MeOH
multiple myeloma	MM
nicotinamide adenine dinucleotide (reduced)	NADH
nicotinamide adenine dinucleotide phosphate (reduced)	NADPH
non-essential amino acid	NEAA
nuclear factor, erythroid derived 2, like 2	NRF2
oxidized glutathione	GSSG
phosphate buffered saline	PBS
positron emission tomography	PET
protein kinase Cζ	PKCζ
radiochemical conversion	RCC
radiochemical purity	RCP
radiochemical yield	RCY
reductive carboxylation	RC
single photon emission computed tomography	SPECT
solid phase extraction	SPE
solute carrier family 1 member 5	SLC1A5
targeted radionuclide therapy	TRT
tert-butoxycarbonyl	Boc
tert-butyl	tBu
thin layer chromatography	TLC
tosyl	Ts
tricarboxylic acid	TCA
trifluoroacetic acid	TFA
tumour microenvironment	TME

1. Introduction

Cancer remains one of the leading causes of death worldwide and its incidence is on the rise despite continuous progress in treatment and research. Methods established in the field of nuclear medicine have a great impact on research, diagnosis, and therapy of cancer, exploiting radioactive decay of nuclides for imaging biomolecular processes and for irradiation of tumour cells. For the development of suitable radiopharmaceuticals for specific targeting of tumour cells while ensuring low exposure of healthy tissue, biological differences of tumour and non-malignant cells need to be studied in detail. Cell metabolism in tumours significantly differs from that of normal mammalian cells. The first has mainly been characterised by an alteration of glycolysis, which has been thoroughly studied and is found in most tumour types. This characteristic is successfully exploited in tumour imaging with positron emission tomography (PET) using the radioactively labelled glucose analogion 2-[^{18}F]-fluoro-2-deoxy-D-glucose (2-[^{18}F]FDG). Later, glutamine started to receive attention as a principal nutrient and target of metabolic reprogramming in malignant cells.[1] While glutamine metabolism lacks a clinically implemented radiotracer, a variety of PET-tracers is used for imaging of different aspects of other metabolic pathways, such as amino acid transport and fatty acid degradation.[2] Developing efficient production methods for PET-tracers can be challenging due to complex syntheses with short-lived radionuclides, in addition to common challenges faced in chemical synthesis of non-radiolabelled pharmaceuticals. However, the establishment of novel radiotracers may allow for a more detailed understanding of complex tumour metabolism and thus aid the development of therapeutic strategies to combat cancer. Moreover, limitations of 2-[^{18}F]FDG in tumour imaging, in particular non-specific uptake due to a variety of non-malignant causes, are further reasons why alternatives are sought.[3]

2. Theoretical Background

2.1 Significance of glucose and glutamine metabolism in tumours

Glucose and glutamine are two main nutrients which cells in higher organisms depend on. Oxidation of their metabolites reduces coenzymes which in turn sustain the electron transport chain with electrons to produce energy in the form of adenosine triphosphate (ATP), as well as nicotinamide adenine dinucleotide phosphate (NADPH), which contributes to redox homeostasis. In addition to glucose providing carbon for biosynthesis of macromolecules,

glutamine is also a source of nitrogen for biosynthesis of nucleotides and nonessential amino acids, and has been shown to facilitate the import of other amino acids.[4]

An increased uptake of glucose in tumour cells compared to normal tissue was first discovered approximately 100 years ago by O. Warburg. Tumour cells can be metabolically reprogrammed to use glucose for aerobic glycolysis instead of oxidative phosphorylation. Thus, lactate is produced in excess, which drives tumour growth. As a consequence, aerobic glycolysis in the presence of oxygen has been referred to as the "Warburg effect" and defines 70-80 % of cancers in humans.[5,6] Initially, Warburg attributed this phenomenon to a loss of mitochondrial function, however more recent hypotheses rather imply that the Warburg effect is a result of metabolic reprogramming of tumour cells. In the majority of tumours, an interplay of several factors sustains aerobic glycolysis. These are based on altered signalling, activation of oncogenes and the transcription factor hypoxia-inducible factor-1 (HIF-1), and impairment of tumour suppressor function.[5] Important examples of altered signalling are the activation of the receptor-tyrosine kinase–PI3K–Akt–mTORC1 pathway and inactivation of the 5' adenosine monophosphate-activated protein kinase (AMPK) pathway. Glucose uptake is also influenced by oncogenes KRAS and BRAF and loss of function of the tumour suppressor mutant p53. The serine/threonine kinase Akt influences localization of glucose transporter GLUT1 at the cell surface and stimulates hexokinase activity and thus glucose phosphorylation. Transcription factor c-Myc increases conversion of glucose-derived pyruvate to lactate.[7]

Glutamine is a non-essential amino acid per definition, as it is produced endogenously. This occurs via amidation of glutamic acid with ammonia, or via transamination and amidation of α-ketoglutarate (α-KG) derived from glucose.[8] However, tumour cells can be characterised by a higher need of glutamine than can be met by endogenous biosynthesis, in which case the amino acid can be considered essential.[9] An increased dependency of tumour cells on glutamine was first reported by H. Eagle in 1956, who found that HeLa cells require it for survival. Following this, in the 1970s, it was found that glutamine is a main player in oxidative metabolism in HeLa cells, hepatoma and lymphoma.[1]

Due to its essential role for tumour cell survival, different aspects of glucose metabolism have been explored as potential targets for cancer therapy. An example with promising results in preclinical studies is 2-deoxy-D-glucose (2-DG). After phosphorylation it is not metabolised further and inhibits general glycolysis in the cell. In vitro, 2-DG has been effective in hindering proliferation in some cancer cell lines, but in vivo assays delivered mixed results, indicating that 2-DG may on the contrary also aid survival of tumour cells. Another potential anticancer

agent that has moved on to clinical trials is Lonidamine. It is suggested to suppress glycolysis by inhibiting hexokinase 2. However, results included high toxicity and a lack of survival benefits for the patients. In combined therapy Lonidamine was more successful, but this was accompanied by high liver and pancreatic toxicity.[10] Glutamine metabolism may be a potential alternative target for therapeutic strategies and several aspects are being explored therefore. These include the inhibition of transporters and metabolic enzymes. Furthermore, the use of glutamine mimics or glutamine depleting agents is being discussed. For most of the drugs that have been developed application is limited due to toxicity, or they merely obtained the status of "preclinical tools". However, glutaminase inhibitor CB-839 has entered several clinical trials. It has shown effective anti-tumour activity in triple negative breast cancer and haematological malignancies in pre-clinical studies.[1]

While the development of therapeutic strategies targeting tumour dependency on glucose has encountered setbacks, this characteristic has been successfully exploited otherwise in nuclear medicine, namely for molecular imaging. The establishment of techniques for imaging glutamine metabolism may aid the prediction of tumour response to therapy targeting glutaminolysis and aid the development thereof.

2.2 Nuclear medicine and imaging

One main technique in molecular imaging is positron emission tomography (PET), which exploits the radioactive decay of radionuclides and is thus attributed to the field of nuclear medicine. For an increased spatial resolution and associating functional with anatomic information PET is coupled with computed tomography (CT), which is based on x-rays, in multimodal scanners.[4] Nuclear medicine refers to the application of radioactive pharmaceuticals in physiological and functional studies of organs and in diagnosis and therapy of a large variety of disorders.[11] The right choice of radiopharmaceutical for a certain clinical application depends on its availability and production costs as well as on multiple physical and biochemical factors. Physical properties include the half-life of the radionuclide, the type and energy of the emission and which daughter nuclides are produced in the decay process. Biochemical considerations are related to in vivo targeting and retention, stability and toxicity.[12] Besides biochemical toxicity of the radiopharmaceutical, the radiation exposure of the patient needs to be evaluated, which is influenced by the effective half-life and the type and energy of the radiation.[13]

The effective half-life is constituted by the physical half-life of the radionuclide and the biological half-life of the radiopharmaceutical. The first refers to the time it takes until half of the radioactivity has decayed. The half-life must be long enough to allow for sufficient remaining radioactivity by arrival at the target after the synthesis of the pharmaceutical and administration to the patient. At the same time, exposure of the patient and the environment must be limited.[12] For successful targeting in therapy and imaging, the biological half-life must fit the physical half-life. The biological half-life is dependent on the time it takes until the molecule reaches its target, its metabolism and rate of excretion (pharmacokinetics). Therefore, dosimetry studies are performed to evaluate the pharmacokinetics with regard to exposure of healthy tissue to radiation.[12]

In general, more metallic than organic radionuclides are available for use in nuclear medicine. Organic radionuclides can directly be attached by covalent bonds or introduced by isotopic substitution to molecules that are directed at a specific target in the organism, in which case the organism cannot differentiate between the radiolabelled and the original molecule. Bifunctional chelating agents are needed to attach radiometals.[14] There are three main classes of compounds used for radiolabelling; small molecules, peptides and antibodies. With increasing size, pharmacokinetics range from fast to slower, and pharmacodynamics are influenced less by radiolabelling with radiometals using chelators.[15] Examples of radiopharmaceuticals used in the clinic with fast kinetics are perfusion tracers that are correspondingly labelled with radionuclides with short half-lives; nitrogen-13 and oxygen-15 (10 and 2 min, respectively), in the form of [^{13}N]ammonia and [^{15}O]water.[16] Longer-lived radionuclides are more prevalent in therapy but are also used in imaging for labelling of antibodies which have slower pharmacokinetics. An example is zirconium-89 with a half-life of 3.3 days, that is used for antibody labelling for PET-imaging.[17]

The type of radiation is another key factor influencing the choice of radionuclide for diagnostic or therapeutic strategies. Alpha- and beta-emitters are suitable for therapy as they have a high linear energy transfer (LET), which refers to ionisation per length of travel. β-emitting radionuclides can additionally emit enough gamma radiation to be made use of in imaging for following the distribution of the pharmaceutical during therapy. Thus far β-emitters have been dominating in radiotherapy. Radiotherapy can take place in form of external beam radiation or targeted radionuclide therapy (TRT), otherwise called endoradiotherapy.[12] Using the same targeting vector for diagnosis and therapy while varying the radionuclide for the respective purpose is referred to as theranostics.[18] With TRT comes the possibility to deliver radioactivity

specifically to the desired target and minimize irradiation of healthy tissue. Examples of common TRT radiopharmaceuticals in clinical use are ^{177}Lu-DOTATATE for neuroendocrine tumours, [^{131}I]iodide for thyroid cancer and Graves' disease and [^{89}Sr]strontium chloride for pain palliation in bone metastasis.[12,18] For therapy with external beam radiation the location of the lesions must be known precisely for selective destruction of tumour cells and avoiding damage of healthy tissue. The location can be determined by anatomic or functional imaging.[13]

Gamma radiation is exploited for imaging in nuclear medicine. This is provided by radionuclides decaying by isomeric transition or electron capture. It can be measured well from outside the body due to a lower LET, an essential aspect for imaging. Another option is the use of positron emitters, as two 511 keV annihilation photons are produced in the collision of a positron with an electron. Single-photon emission computed tomography (SPECT) and positron emission tomography (PET) are the techniques that exploit these two types of radiation sources, respectively, for visualizing biochemical processes in the body.[19] The γ-emitter that is used the most in SPECT is technetium-99m for diagnosis of disorders of the brain, liver and heart, among others.[13] Iodine-123 is another SPECT radionuclide, used as a diagnostic marker for disorders of the thyroid. Another radiometal that is common in PET-tracers is gallium-68 with a half-life of 68 minutes. Its production is convenient as it is available from a radionuclide generator by decay of germanium-68, however radiolabelling via a metal-ligand complex is necessary and this changes the molecule to a higher extent.[14] Its major application is in the form of radiolabelled peptides ^{68}Ga-DOTATOC, ^{68}Ga-DOTATATE and ^{68}Ga-DOTANOC, which target somatostatin receptors that are overexpressed in different types of neuroendocrine tumours.[20] The use of gallium-68 labelled peptides for diagnosis and following with therapy using the ^{177}Lu- or ^{90}Y-labelled tracer equivalents is a classic example of theranostics.[18] Radiopharmaceuticals in PET based on small molecules are labelled with non-metal radionuclides such as fluorine-18 and carbon-11. Carbon-11 is used especially for brain imaging, labelling amino acids and other metabolic tracers such as [^{11}C]acetate used in cardiology and prostate cancer imaging.[14] From all metabolic tracers, the working horse of PET however is 2-[^{18}F]-fluoro-2-deoxy-D-glucose (2-[^{18}F]FDG), which accounts for approximately 95 % of PET studies (by 2020).[21]

2.3 2-[^{18}F]FDG-PET/CT and its limitations

The first in human trial of 2-[^{18}F]FDG was conducted in 1976, and until the early 1990s the radiotracer was used in academic settings, mainly for studying the brain. From then on, its clinical use increased drastically, also owing to a higher number of cyclotrons available for

production and shipping to other sites. Over time, a variety of application fields was discovered, the main being oncology.[21] The success of 2-[^{18}F]FDG as a PET-tracer depends on various factors: fluorine-18 has advantageous physical properties, as it is an essentially pure positron emitter, with low positron energy. This results in a short length of travel within cells, which in turn is positive for spatial resolution. Due to a lack of fluorine in natural biomolecules, isotopic substitution is not possible, which would be ideal for maintaining pharmacological properties. Nonetheless, as the atom is small and molecules can be labelled directly with this radionuclide, structural changes are minimal compared to labelling with radiometals.[22] The applicability of 2-[^{18}F]FDG-PET in oncology is due to an increased rate of glucose consumption in many types of malignant cells, already demonstrated by Otto Warburg early in the last century. Based on these metabolic alterations 2-[^{18}F]FDG-PET allows for differentiation between normal and cancerous tissue.[23] The increased need for glucose in tumour cells is met by upregulation of glucose transporters GLUT1 and GLUT2 and hexokinase activity.[22] Equally to glucose, 2-[^{18}F]FDG is phosphorylated by hexokinases. It has been considered to thus be metabolically trapped, due to slow dephosphorylation to be able to exit the cell, ascribed to low levels of the corresponding enzyme.[23] Nevertheless, its exact mode of action remains unclear and recently it was shown that 2-[^{18}F]FDG is metabolised also beyond phosphorylation.[24] Apart from oncology, 2-[^{18}F]FDG-PET is also implemented in cardiology and neurology, for example for imaging energy turnover of the cardiac muscle and evaluating dementia[14] as well as in infection and inflammation.[25]

The extensive and diverse application of 2-[^{18}F]FDG also bears disadvantages for tumour imaging. High background glucose uptake can hinder the effective distinction of tumour and healthy tissue, which is especially the case for malignancies located in the brain. This is why 2-[^{18}F]FDG has been discussed to be ineffective for imaging gliomas.[26] There are non-malignant causes for uptake that include a number of benign tumour types, and there are indications for the use of 2-[^{18}F]FDG in imaging of infection and inflammation.[25] The reason for this is that 2-[^{18}F]FDG uptake in the tumour microenvironment (TME) is not solely ascribed to tumour cells, but also to inflammatory cells surrounding them, such as activated macrophages, which may even exhibit a higher uptake. This is an important consideration especially for chemotherapy patients that are more prone to infections.[3,27] This phenomenon can cause an apparent disease progression in the case of immunotherapy, referred to as “pseudoprogression”, due to high immune stimulation and recruitment of immune cells to the TME during the first stages of treatment, for example in the case of lymphoma treatment using rituximab.[28,29] The Warburg effect is not limited to tumour cells but can also occur in immune cells upon infiltrating the

TME, as they need to adapt their metabolism due to nutrient deficiencies in the harsh environment in the TME.[30] Thus, there is a competition between these two cell types for both glucose and glutamine in a shared pool in the TME. It has been shown in different tumours that the highest glucose uptake in the TME is in immune cells and that of glutamine is in tumour cells. These findings suggest that 2-[^{18}F]FDG-PET images may be influenced by tumour infiltrating immune cells which may provide an explanation for regional uptake variation.[31] The existence of 2-[^{18}F]FDG-negative tumour types, as well as tumours with insufficient uptake for reaching the desired sensitivity, also calls for alternative radiotracers. Examples are certain types of hepatomas, tumours in the gastrointestinal tract, renal cell carcinomas and lymphomas. Furthermore, the majority of advanced breast cancer cases is associated with bone metastases. While 2-[^{18}F]FDG-PET is efficient for detecting osteolytic breast metastases, sclerotic bone metastases are not diagnosed.[3]

Non-specific uptake in myocardium, muscle and fatty tissue is possible and ascribed to glucose transporter 4 expression in these tissues. In skeletal muscle, uptake is enhanced significantly by the patient exercising before 2-[^{18}F]FDG administration. This can also occur through muscle activation due to stress. In addition, the use of insulin shortly before the PET-scan also drives skeletal muscle uptake. Brown adipose tissue (BAT) is also well known to display non-specific uptake. It is abundant in new-borns and occurs in lower amounts in adults, with higher prevalence in women and people with low body mass index.[3] While it is usually found around the neck and above the clavicula, risk of misinterpretation mainly occurs in the case of atypical location of brown fat.[25,32] Its function is thermogenesis, triggered by cold temperature and food ingestion, which means that keeping the patient warm and special dieting before the scan may be necessary to restrict glucose influx into BAT and increase 2-[^{18}F]FDG uptake in malignancies.[32]

To summarize, there are several sources of potential misinterpretation of images obtained with the PET-tracer gold standard 2-[^{18}F]FDG. On the one hand, non-specific uptake can lead to false-positives in tumour imaging and on the other hand there are 2-[^{18}F]FDG-negative lesions that this imaging technique fails to detect.

2.4 Metabolic imaging in tumours

Thus, the development of further radiotracers for PET-imaging of various metabolic pathways is desirable. A selected number of existing tracers and their application shall be mentioned here. 14-(R,S)-[^{18}F]-fluoro-6-thiaheptadecanoic acid ([^{18}F]FTHA) can be used to evaluate fatty acid

metabolism. This can also be done via another tracer, [^{11}C]palmitate, which has the advantage of isotopic labelling, meaning it has the same metabolic fate as the non-labelled free fatty acid. High proliferation rates in tumours call for imaging techniques based on nucleoside metabolism. [^{18}F]fluorothymidine ([^{18}F]FLT) has been developed for this purpose and has been used for lung, breast, and colon cancer staging. Though as it shows lower uptake than 2-[^{18}F]FDG it is more suitable for assessing treatment response. Due to generally high metabolic rates and nutrient consumption of tumour cells, labelling amino acids and assessing uptake by their corresponding membrane transporters, which are often overexpressed, is a much-explored strategy. Examples are [^{11}C]methionine ([^{11}C]MET) and [^{11}C]tyrosine in brain tumours, as well as [^{18}F]fluoroethyltyrosine ([^{18}F]FET). [^{18}F]FET and 6-[^{18}F]fluoro-L-3,4-dihydroxyphenylalanine ([^{18}F]FDOPA) target the large amino acid transporter (LAT1), which is overexpressed in some tumours such as pancreatic and lung carcinomas.[2] As mentioned, metabolism of glutamine is, next to glycolysis, a major aspect that is reprogrammed and amplified in cancer cells. This explains why there is a significant interest in establishing an imaging technique that is based on this amino acid.

2.5 Glutamine metabolism

As discussed, despite the success and widespread use of 2-[^{18}F]FDG-PET, there are some scenarios in which its application is not suitable. Enhanced glycolysis and lactate secretion (Warburg effect) is only one aspect of the altered metabolism of cancer cells and has in fact been shown to be insufficient for cancer cell survival by itself. The other source of energy that can be affected is mitochondrial metabolism, via the tricarboxylic acid cycle and oxidative phosphorylation, which are driven by glutamine, making it a highly interesting target in tumour imaging.[33–35] Besides being used for protein and nucleotide biosynthesis, glutamine is involved in the biosynthesis of glutathione (GSH) and nonessential amino acids (NEAAs), and provides anaplerosis, sustaining the tricarboxylic acid (TCA) cycle.[36]

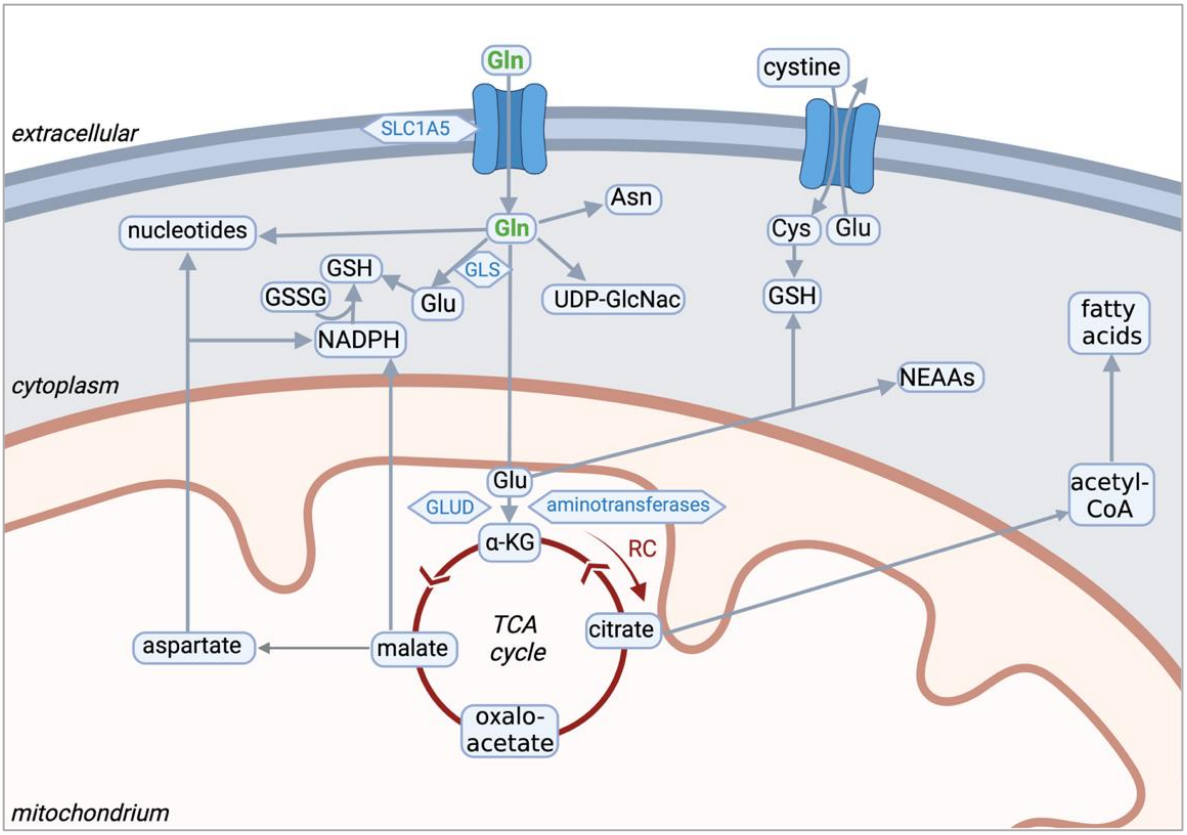

Figure 1: Overview of glutamine metabolism in the cell. Created with BioRender.com, adapted from Yoo et al. and Altman et al.[1,9] For abbreviations and corresponding full forms see text and List of abbreviations.

Nucleotide biosynthesis is pivotal for fast proliferation and glutamine provides the essential nitrogen. Five glutamine amide nitrogen atoms are needed in total for purine and pyrimidine biosynthesis.[37] In addition to that, aspartate, created in the conversion of glutamine to glutamate, is involved in several steps in the nucleotide biosynthetic pathway.[36] Apart from nucleotides, glutamine in the cytoplasm is used to produce hexosamines, asparagine (Asn) and glutathione. Glutathione consists of glutamate, cysteine (Cys), and glycine. Glutamine can be converted to phosphoserine and α-KG, and these to glycine, and there is an exchange mechanism between glutamate and cystine, which is reduced to cysteine in the cell.[1] Nitrogen from glutamine-derived glutamic acid is used in the production of serine, alanine and aspartate. Its carbon and nitrogen can be incorporated into proline, ornithine and arginine.[37] In vitro experiments have shown that a minimum of 50 % of non-essential amino acids used for protein biosynthesis in cancer cells originate from glutamine.[1]

In the mitochondria glutamine is converted to glutamate by amidohydrolases (GLS, GLS2). Glutamate that is not exported to the cytosol is further metabolised by glutamate dehydrogenase (GLUD) or aminotransferases to α-KG, which is introduced into the TCA cycle, generating

energy for the cell. The TCA cycle provides guanosine triphosphate (GTP), which is converted to ATP, and nicotinamide adenine dinucleotide (NADH) and flavine adenine dinucleotide ($FADH_2$). NADH and $FADH_2$ enter the electron transport chain to produce ATP as well, by oxidative phosphorylation. Citrate is utilized for fatty acid biosynthesis in the cytosol. Aspartate is another metabolite that is exported from mitochondria and is pivotal in hypoxic conditions and for NADPH generation, which is needed for reduction of oxidized GSH (GSSG).[36]

2.6 Metabolic reprogramming of tumour cells toward "glutamine addiction"

Tumour cells can be genetically reprogrammed to a higher glutamine dependency. An important example are c-MYC-driven cancers. c-MYC belongs to the MYC oncogene family, which regulates the expression of a lot of different genes whose products influence cell growth, metabolism, differentiation and more, promoting tumour progression.[38] It has been suggested that cells transformed by MYC are unable to use glucose to sustain the tricarboxylic acid cycle, even in cases with high glucose availability, and instead depend on glutamine to maintain it. This has been linked to the progression of lymphomas, neuroblastoma, and small cell lung cancer in humans. The oncogene is responsible for the expression of enzymes involved in nucleotide biosynthesis; direct transcriptional regulation is exercised by c-MYC for three out of five of the glutamine-using biosynthetic steps. It induces increased glutaminolysis through higher expression of glutamine transporters and metabolising enzymes, such as glutaminase, which catalyses the conversion of glutamine to glutamic acid. One of the transporters, SLC1A5, takes part in mTOR complex 1 (mTORC1) activation by exchange of glutamine with essential amino acids, especially leucin, from the extracellular environment, which then directly activate mTORC1. This is a protein complex involved in metabolic reprogramming of cancer cells supporting cell growth.[36,37] SLC1A5 is also induced by K-Ras, another example of an oncogene known to boost glutamine uptake. K-Ras also causes an increased translation of enzymes that catalyse aspartate and α-KG synthesis, contributing to nucleotide biosynthesis and ATP generation.[36] A transcription factor that plays an important role in cancer progression is HIF-α, especially under hypoxic conditions. HIF-1α leads to higher levels of glucose metabolizing enzymes and transporters, and lactate production. Lactate stabilizes HIF-2α, which transactivates MYC. Furthermore, it has been found that HIF-2α regulates SLC1A5 expression in hypoxia.[36,39] Thus, Glutamine uptake is increased in hypoxic conditions. By reductive carboxylation (RC) of α-KG after the conversion of glutamine, citrate is generated, which is used in the cytosol for lipid biosynthesis. This makes up for reduced citrate production in the TCA cycle by lower input of pyruvate due to increased lactate production. This alternative

citrate source has been shown to be essential for the survival of clear cell renal cell carcinoma.[36] There is a number of further influences which includes tumour suppressor p53 driven activation of GLS2 expression, NRF2 (nuclear factor, erythroid derived 2, like 2) promotion of GSH production from glutamine, and JAK2-V617F mutation and protein kinase Cζ (PKCζ) loss that increase glutamine metabolism through GLS activation and serine synthesis, respectively.[1]

2.7 (2S,4R)-[^{18}F]4-fluoroglutamine synthesis

Qu et al. first reported the synthesis of optically pure [^{18}F](2S,4R)-4-fluoroglutamine in 2011.[40] To achieve this, several challenges had to be overcome. Fluorine and carboxylic groups are electron withdrawing, which can promote the epimerisation of positions 2 (α-amino group) and 4, the position of the introduced label, throughout the synthesis. Basic conditions further promote epimerisation of the α-amino group. The amide group can hydrolyse, converting glutamine to glutamic acid. Glutamine and glutamate can cyclize to pyroglutamic acid, in this case yielding 4-fluoropyroglutamic acid, that has been reported as a common impurity in the preparation of the radiotracer. When radiolabelling via bi-molecular nucleophilic substitution (S_N2), elimination of the tosylate group can occur, with reaction temperature and basicity having a significant influence. Furthermore, considering the half-life of fluorine-18, the possible duration of the overall synthesis is limited, and the label should ideally be added towards the end to allow for enough time for in vivo application of the product.

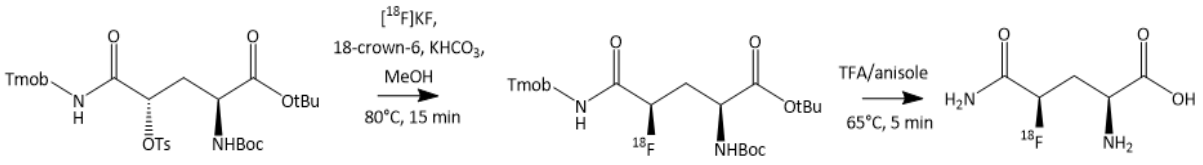

Figure 2: Overview of reaction steps in (2S,4R)-[^{18}F]4-fluoroglutamine synthesis. With Tmob=2,4,6-trimethoxybenzyl, Ts=tosyl, Boc=tert-butoxycarbonyl, tBu=tert-butyl, MeOH=methanol, TFA=trifluoroacetic acid

Qu et al. also described the synthesis of (2S,4S)-tert-butyl-2-(tert-butoxy-carbonylamino)-5-oxo-4-(tosyloxy)-5-(2,4,6-trimethoxybenzylamino)-pentanoate). This (2S,4S)-tosylate precursor for [^{18}F]4-FGln synthesis is now commercially available and can be used directly for fluorination (Figure 2). The first step is the separation of [^{18}F]fluoride from the oxygen-18 water, which radionuclide production at the cyclotron delivers, which is achieved using an ion exchange cartridge. 18-crown-6 as a neutral phase transfer catalyst and $KHCO_3$ as a mild base for elution of [^{18}F]fluoride have been established by Qu et al. as better alternatives to the commonly used Kryptofix® 222 and K_2CO_3, as that standard method led to formation of all

stereoisomers in the reaction mixture.[40] Further optimization was achieved by using methanol instead of acetonitrile, improving elution according to X. Zhang et al.[41] This is followed by azeotropic drying with acetonitrile to ensure dry conditions for the addition of the precursor and for the reaction. The reaction mixture containing the radiolabelled intermediate needs to be purified in order to remove unreacted [^{18}F]fluoride and other radiochemical impurities. The second reaction step is constituted by global acidic deprotection yielding (2S,4R)-[^{18}F]4-fluoroglutamine.[40]

2.8 Potential application of (2S,4R)-[^{18}F]4-fluoroglutamine

Glutamine is a nonessential amino acid, but it is considered essential in cancer cells, as they have a higher requirement than can be met by endogenous biosynthesis, which leads to the assumption that a distinction between tumour cells and normal tissue by means of a glutamine-based PET-tracer should be feasible. Renal cell carcinoma, glioblastoma, blood and pancreatic adenocarcinoma are examples for cancers that are known to depend on glutamine.[26,36] As discussed, using a PET-tracer based on glutamine may be preferrable to 2-[^{18}F]FDG in some cases and can be used to investigate glutamine metabolism and potentially detect specific genetic changes and hypoxia, which may be relevant for determining adequate, personalised treatment. Since Qu et al. published the above-mentioned synthesis method[40], several in vitro and in vivo studies have been conducted, assessing metabolism of the radiotracer and uptake in glutamine-addicted tumour cells and mouse models. The first studies included [^{18}F]4-FGln uptake assays in the 9L tumour cell line, and SF188-Bcl-$_{xL}$ tumour cells with up-regulated c-MYC gene, thus “glutamine-addicted”, by Qu et al. and Lieberman et al. These demonstrated a higher [^{18}F]4-FGln than 2-[^{18}F]FDG uptake in the latter, providing first indications for the feasibility of the application of this radiotracer as an alternative to the gold standard in tumour imaging.[40,42] N-MYC-amplified neuroblastoma has also been shown to prefer [^{18}F]4-FGln over 2-[^{18}F]FDG and displayed higher uptake of [^{18}F]4-FGln compared to neuroblastoma without this genetic transformation. N-MYC-amplification is connected to worse prognosis due to aggressiveness of the tumour. Thus, the authors discuss [^{18}F]4-FGln-PET as a valuable tool to distinguish between the two types, aiding therapy planning, as characteristics of N-MYC-amplified tumours may be potentially targeted in treatment.[43] Valtorta et al. reported that in some cases, multiple myeloma (MM) can be 2-[^{18}F]FDG-PET negative and MM cells are glutamine addicted, characterised by high expression of glutamine transporters and uptake of the amino acid from the TME. The authors also discuss that [^{18}F]4-FGln can be helpful to study

the metabolism of MM to determine differences among cell subpopulations, to assess response to therapy, and for designing new therapies targeting specific metabolic characteristics.[44]

First in-human experiences have been reported in recent years which have yielded valuable information about the potential application of the novel PET-tracer and its metabolic fate in vivo. [^{18}F]4-FGln has been shown to be taken up more specifically in gliomas and to result in a more efficient demarcation of the tumours in the brain than 2-[^{18}F]FDG, which has a higher background uptake.[26] Nevertheless, for glioma imaging alternative tracers based on amino acid targeting the LAT1 transporters, that are overexpressed in high grade gliomas, are already well established, such as [^{11}C]MET and [^{18}F]FET.[45] PET assays by Dunphy et al. included patients with different cancer types which were successfully depicted by [^{18}F]4-FGln-PET. This was especially the case for aggressive tumours with genetic alterations affecting glutamine metabolism and included tumours in the breast, kidneys, pancreas, colon, and lung. In addition, they compared bone uptake in [^{18}F]4-FGln-PET and [^{18}F]sodium fluoride ([^{18}F]NaF)-PET and observed half as much uptake of label than with the latter, without impeding the detection of metastases in the bones.[46]

To summarize, considering the limitations of the PET gold standard 2-[^{18}F]FDG and the enhanced metabolic contribution of glutamine in certain tumours, radiolabelled glutamine may be a suitable candidate for an alternative metabolic tracer for application in PET.

3. Aim and Hypothesis

Glutamine is, besides glucose, a principal nutrient for cancer cells, generating energy and providing carbon and nitrogen for macromolecule biosynthesis. Several tumour cell types even exhibit a higher dependency on or “addiction” to glutamine due to metabolic reprogramming. Therefore, radiolabelling this amino acid has a lot of potential for assessing tumour metabolism via PET/CT and serving as an alternative to the well-established 2-[^{18}F]FDG. This is relevant due to limitations of the latter for certain applications, but also the potential to predict genotypes or hypoxia from a [^{18}F]4-FGln scan, which may be relevant for the exploration of new therapeutic strategies. Successful synthesis of [^{18}F]4-FGln has been reported before and automated synthesis has been established on different radiosynthesis modules.

The first aim of this work is to set up a reliable automated synthesis on an ELIXYS FLEX/CHEM automated synthesizer, including a purification method for the intermediate and suitable quality control methods. Based on the reference literature we hypothesize that radiosynthesis of [^{18}F]4-FGln is achievable with sufficient radiochemical yield, as well as

radiochemical and stereochemical purity for in vivo application in the future. The second aim is the evaluation of in vitro [^{18}F]4-FGln uptake in two tumour cell lines and comparison to the PET gold standard 2-[^{18}F]FDG, as well as [^{3}H]Gln as a reference. Due to the Warburg effect and the role of glutamine as another primary nutrient in tumour cells, it is expected that the uptake of all radiotracers is significant.

4. Materials and Methods

4.1 Production of (2S,4R)-[^{18}F]4-fluoroglutamine

4.1.1 General

Unless otherwise stated, all chemicals were commercial products and used without further purification. Water was purified with a Milli-Q® Direct 8 water purification system from Merck Millipore before use. Phosphate buffered saline (PBS, pH=7.4) was obtained from MORPHISTO GmbH (Offenbach am Main, Germany). The precursor for the [^{18}F]4-FGln synthesis, (2*S*,4*S*)-*tert*-butyl-2-(*tert*-butoxy- carbonylamino)-5-oxo-4-(tosyloxy)-5-(2,4,6-trimethoxybenzylamino)-pentanoate, was purchased from ABX advanced chemical compounds (Radeberg, Germany) and from Memorial Sloan Kettering Cancer Center (New York, USA). Non-radioactive standard 4-FGln was also purchased from the latter. The precursor was stored long-term at -80°C under inert atmosphere. For short-term storage it was kept at -20°C under inert atmosphere. Chromafix® PS-HCO^{3-} cartridges were obtained form Macherey-Nagel (Düren, Germany, Lot No. 96.038). Oasis® HLB Light cartridges were purchased from Waters (Milford, MA, USA, Lot No. 125B35222A). Syringes and needles were obtained from B. Braun Melsungen AG (Melsungen, Germany). Millex® filter units were obtained from Merck Millipore Ltd. (Cork, Ireland).

[^{18}F]fluoride was produced via the ^{18}O(p,n)^{18}F reaction on the in-house GE PET-TRACE 800 cyclotron. Typically, between 6 and 15 GBq were produced with a 55 µA beam current. To obtain low activities needed for small scale manual syntheses, normally between 90 and 150 MBq, the target was flushed with [^{16}O]H_2O after routine 2-[^{18}F]FDG syntheses without additional radiation.

The elution efficiency of [^{18}F]fluoride from Chromafix® PS-HCO_3^- cartridges using 0.18 mL $KHCO_3$ (8 mg/mL) in 1 mL 18-crown-6 in MeOH (8 mg/mL) was assessed by measuring the trapped and eluted radioactivity with a dose calibrator.

[^{18}F]4-FGln was synthesized using an ELIXYS FLEX/CHEM automated synthesizer and PURE/FORM automated radiopharmaceutical HPLC purification and formulation platform and ELIXYS software by SOFIE Biosciences (Culver City, California, USA). Two methods for purification via semi-preparative HPLC were established. The first included a SUPERCOSIL™ LC-ABZ+ 250 x 10 µm, 5 µm column (Supelco™ Analytical, Cat# 59179) with a 20-90 % acetonitrile (ACN)/water gradient within 30 min at a 5 mL/min flow rate. In the second method purification was done with isocratic MeOH/water (8:2) mixture + 0.1 % formic acid at 5 mL/min flow, using a Gemini® 5 µm C18 110 A 250 x 10 mm column (Phenomenex, Part No. 00G-4435-NO).

4.1.2 Module preparation

A Chromafix® PS-HCO_3^- cartridge was placed in-between the designated fittings of cassette 1. An Oasis® HLB Light cartridge was conditioned with 5 mL EtOH, 10 mL air and 10 mL water and mounted onto the PURE/FORM unit. The output line of cassette 1 was connected with the PURE/FORM input line for transfer to the HPLC system. A Falcon™ tube was filled with 6 mL of water and the rinse line of the purification unit placed into the tube. The elute line was placed into a Falcon™ tube filled with a minimum of 3 mL of ethanol (EtOH). The dilution reservoir was filled with 18 mL of water. A product vial was prepared and connected to the output line of cassette 2 via a 0.22 µm, 33 mm sterile filter. A 18G needle with a 0.22 µm, 13 mm sterile filter was added to the product vial for ventilation. The cold trap was filled with EtOH and dry ice.

0.18 mL $KHCO_3$ (8 mg/mL) and 1 mL 18-crown-6 in MeOH (8 mg/mL) were filled into vial 1.1 (cassette 1, vial 1). Vials 1.2 and 1.3 were each filled with 1 mL ACN. Vial 2.1 (cassette 2, vial 1) was filled with 1 mL of trifluoroacetic acid (TFA) and 10 µL anisole. 1 mL of EtOH was added to vial 2.2. Vials 2.3 and 2.12 were filled with 1 and 2 mL of PBS, respectively. 5 mg of precursor were brought to room temperature and just before the start of the synthesis dissolved in 0.6 mL acetonitrile and added to vial 1.4. The activity line of cassette 1 and the delivery gas line were connected to the irradiation vial after [^{18}F]fluoride production.

4.1.3 Radiosynthesis

4.1.3.1 Fully automated HPLC-based synthesis

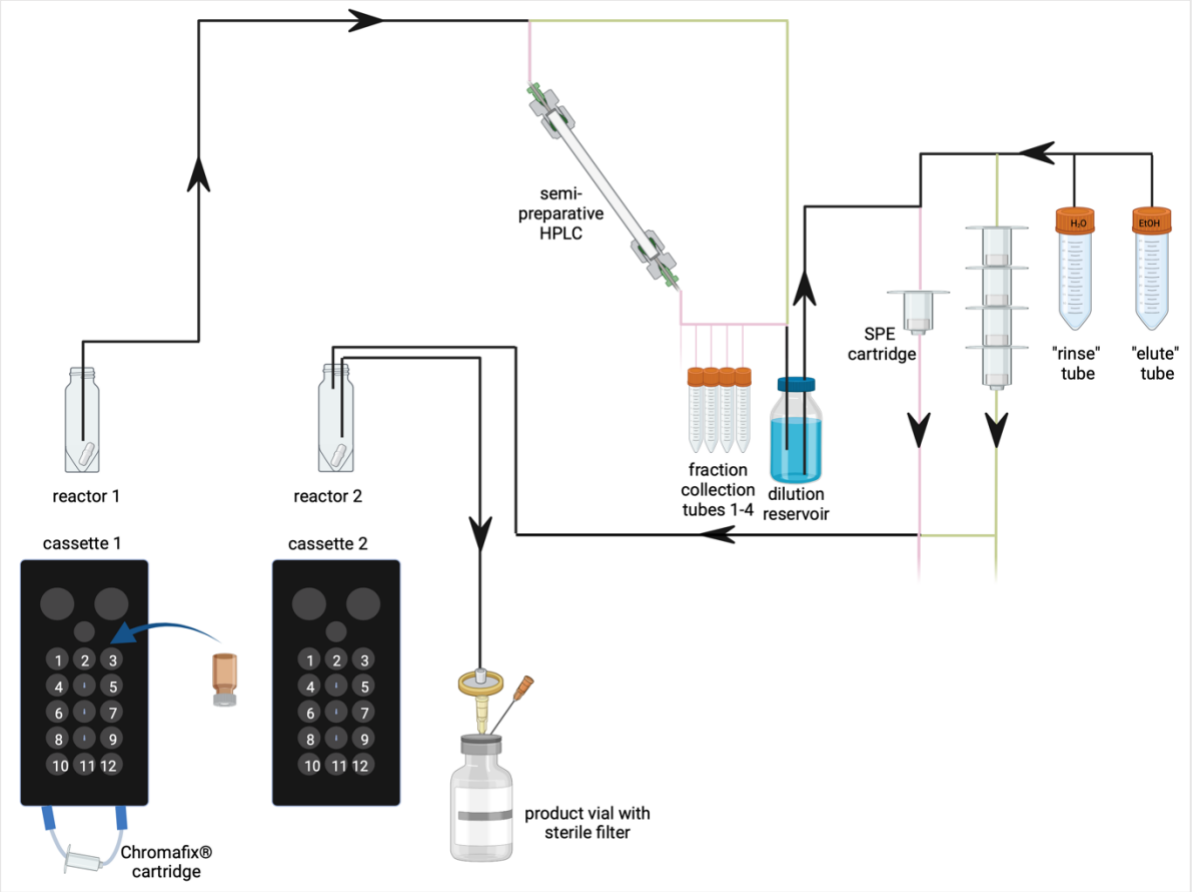

Figure 3: Scheme of the automated synthesis on the ELIXYS module, created with BioRender. Pink path refers to purification via semi-preparative HPLC, green path shows alternative flow when using cartridges only. Fading lines indicate waste path.

[^{18}F]fluoride was trapped on a Chromafix® PS-HCO_3^- cartridge (3 min) and eluted with 0.18 mL $KHCO_3$ (8 mg/mL) in 1 mL 18-crown-6 in MeOH (8 mg/mL) into reactor 1 (3 min). 1 mL of ACN was added (2 min), and this was evaporated at 90°C under argon/vacuum (8 min), then cooled to 35°C. Again 1 mL of ACN was added (2 min) and evaporated at 90°C (8 min), then cooled to 45°C. 5 mg of precursor dissolved in 0.6 mL ACN were added and the reaction mixture stirred at 80°C (15 min), then cooled to 35°C. 2.4 mL of water (or 2.4 mL of mobile phase in semi-preparative purification method 2) were added and the mixture was transferred to the PURE/FORM purification unit. The intermediate was eluted after 21-22 minutes for the first method and after 6-7 minutes for the second method and collected in the pre-filled dilution reservoir. The contents of the dilution reservoir were trapped on a preconditioned Oasis® HLB light cartridge. The cartridge was rinsed with 6 mL of water and the intermediate eluted with

2.5 mL of EtOH into reactor 2. The total duration of the formulation was 15 minutes. EtOH was evaporated at 65°C (7 min). 10 µL anisole in 1 mL TFA were added and the mixture heated at 65°C for 5 mins, then evaporated at 65°C (4 min). 1 mL of EtOH was added and evaporated at 65°C (7 min). 2 mL of PBS (pH 7.4) were added and the contents of reactor 2 transferred through a sterile filter into a product vial. Then 1 mL of PBS was added into reactor 2 and again transferred to the product vial. All above mentioned reaction and evaporation steps were conducted whilst stirring with a magnetic stir bar. The total sequence run time added up to 2 hours for purification method 1 (1h55min), and the duration was 15 minutes less for the sequence with the second purification method.

4.1.3.2 Fully automated cartridge-based synthesis

For the modified purification involving cartridges only (Figure 3), the reaction mixture with the intermediate was diluted with 2.4 mL of mobile phase after the reaction and transferred over the PURE/FORM HPLC system directly into the dilution reservoir, prefilled with 60 mL of water. The contents of the dilution reservoir were trapped on 4 consecutive pre-conditioned Oasis® HLB Light cartridges and washed with 10 mL of water. 5 mL of EtOH were used for elution of the intermediate into reactor 2. The duration of the synthesis using this purification method was 1 hour 40 minutes.

4.1.3.3 Small scale synthesis

For manual small-scale syntheses of the intermediate, normally between 90 and 150 MBq of [^{18}F]fluoride were trapped on a Chromafix® PS-HCO_3^- cartridge and then eluted with 0.18 mL $KHCO_3$ (8 mg/mL) in 1 mL 18-crown-6 in MeOH (8 mg/mL) into a reactor with a stir bar on a magnetic stirrer. Azeotropic drying was achieved by twice adding 1 mL of ACN under N_2 and evaporating at approximately 75°C. While keeping the reactor closed and under an N_2 atmosphere, 0.1-1 mg of precursor in 0.6 mL ACN were added and reacted for 15 mins at 80°C. The reaction mixture was diluted with 2.4 mL water and the conversion to the intermediate was determined with the established HPLC method.

4.2 Quality control of radiolabelled intermediate and [^{18}F]4-FGln

Radiochemical purity of the intermediate and of the product were determined on a HITACHI Chromaster System with a GINA Star 5.9 software, 5160 pump, 5310 column oven and a Raytest Gabi Star radioactivity detector. Absorbance was measured at 254 nm with a 5410 UV detector. A Gemini® 5 µm C18 110 Å LC 250 x 4.6 mm column (Phenomenex, Part No. 00G-

4435-E0) was operated at room temperature with MeOH/water (8:2) mixture + 0.1 % formic acid as a mobile phase, with a 1 mL/min flow rate. Residual anisole can also be determined with this HPLC method (t_R~4.5 min).

Radiochemical purity and stereochemical purity of the product were determined by co-injecting with non-radioactive standard 4-FGln on a Chirex® 3126 (D)-penicillamine 150 x 4.6 mm column (Part No. 00F-3126-E0, Phenomenex,) with 1mM $CuSO_4$ as the mobile phase with a 1 mL/min flow rate, at room temperature. It was operated on a Shimadzu HPLC system with a CBM-20A communications bus module, DGU-20A5R degassing unit, LC-20AD pump, and GINA Star software (version 10.4). A RamonaStar radioactivity detector and SPD-M20A photo-diode array detector was used for UV measurement at 254 nm.

Thin layer chromatography (TLC) was conducted on silica using a 2-propanol/acetic acid/water (3:1:1) mixture as a mobile phase. For amino acid detection a ninhydrin solution consisting of 0.2 g ninhydrin and 0.5 mL acetic acid in 100 mL acetone was applied, with subsequent heating. Fluorine-18 was detected with a Gita star raytest detector (Elysia Raytest, software version 6.3).

4.3 Cell culture and cell uptake assays

4.3.1 Material

Gibco™ RPMI Medium 1640 (1x), 500 mL; Minimum Essential Medium (MEM (1x)), 500 mL; Dulbecco's Modified Eagle Medium (DMEM (1x)), 500 mL; Dulbecco's phosphate buffered saline (DPBS), without calcium, without magnesium, 500 mL; 0.05% trypsin-EDTA (1x), 100 mL, and fetal bovine serum (FBS) were all obtained from Thermo Fisher Scientific (Waltham, MA, USA). CELLSTAR® sterile cell culture flasks 250 mL, 75 cm^2, PS (Greiner Bio-One GmbH, Frickenhausen, Germany) and BioLite 175 cm^2 vented flasks, (Thermo Fisher Scientific, Rochester, NY, USA) were used for cell cultivation. Cells were incubated in a Thermo electron corporation incubator. Cells were counted on a LUNA™ Automated Cell Counter from BioCat with LUNA™ Cell Counting Slides with Trypan blue, 0.4% solution, liquid, sterile filtered from SIGMA Aldrich (St. Louis, MO, USA). 50 mL Falcon™ Polypropylene Conical Tubes, 30 x 115 mm (Corning Science México) were used for centrifuging in a Rontanta 460 RC Hettich centrifuge. Cell Scrapers, PE Blade, PS Handle, 32 cm (large), were obtained from Thermo Fisher Scientific (Mexico). MultiScreen® filterplates DV, 0.65 µm, clear, hydrophilic PVDF, and vacuum pump were obtained from Merck Millipore Ltd. (Darmstadt, Germany). A PerkinElmer Wizard 2 gamma counter was used for measuring samples containing fluorine-18, using 5 mL tubes, 75 x 12 mm, PP, from Sarstedt AG & Co.

KG (Nümbrecht, Germany). Samples containing tritium were measured on a HIDEX 300SL Automatic TDCR Scintillation Counter (Turku, Finland) with a MikroWin Software, Version 4.44, using ULTIMA GOLD™ scintillation cocktail (PerkinElmer, Waltham, MA, USA, Lot No. 77-22041, 5L) in miniature 6 mL polyethylene vials from PerkinElmer (Waltham, MA, USA).

L-[3,4-^{3}H]glutamine 37 MBq/mL in 2% ethanol (ART2306) was received from Hartmanns Analytics, Braunschweig, Germany. 2-[^{18}F]FDG was obtained from the routine in house production at the University Hospital Vienna, Austria.

4.3.2 General

RPMI Medium 1640 (1x) with L-glutamine and 10% FBS was used for cultivating the HT29 cell line. MEM (1x) with Earle's Salts, NEAA, 2 mM L-Glutamine and 10% FBS was used for cultivating the HT1080 cell line. DPBS was used for washing cells and for diluting radioactivity for uptake assays. 0.05 % trypsin-EDTA (1x) was used for detaching cells. MEM (1x) with Earle's Salts, NEAA, without glutamine and FBS was used for [3,4-^{3}H]glutamine uptake experiments. DMEM (1x) without glucose and FBS was used for 2-[^{18}F]FDG uptake experiments. Culture media and trypsin were kept sterile at 2-8°C, DPBS at room temperature. Uptake media were stored not sterile at 2-8°C.

Both cell lines were generally cultivated in 75 cm^{2} sterile flasks, at 37°C and 5 % CO_2. Medium (11 mL) was changed every 1-2 days. Cells were usually split when 80-90% confluent. For this, medium was removed, and the cells were washed with 5 mL of DPBS. 2 mL of 0.05 % trypsin-EDTA were added, and the flask incubated at 37°C for 3-5 minutes until cells were detached. 5 mL of culture medium was added to the trypsin and the 7 mL transferred to a falcon. 10 µL of cell suspension were removed and diluted with 10 µL of trypan blue for cell counting on a LUNA™ cell counter. The cell suspension in the falcon was centrifuged at 1200 RPM and room temperature for 4 minutes. The medium was decanted, and the cell pellet resuspended in medium, and a fraction transferred to a new flask.

4.3.3 Uptake assay in 6-well-plates ("uptake assay I")

HT29 and HT1080 cells (300.000 cells per well) were seeded in 6-well-plates 2 days before the experiment. The medium was removed from the wells, and each well washed with 1 mL DPBS. 1 mL of uptake medium was added to each well. Between 30 and 70 kBq 2-[^{18}F]FDG was pipetted to each well, the same activity was used for each well within one experiment. The plates were incubated for 60 mins at 37°C. The supernatant of each well was transferred to a

gamma counter tube, 1 mL of DPBS was used to wash each well and added to the supernatant. 1 mL of trypsin added to each well and the plates were incubated until the cells were detached. The cell suspensions were transferred to gamma counter tubes and 1 mL of DPBS used for washing each well and was added to the suspensions. For each cell line the cells of 2 wells were counted and the average used to normalize the activity to the cell number per well for the cell lines. The tubes were measured on the gamma counter for 30 seconds each. A reference with the total initial activity was also measured.

The uptake assay was performed accordingly with [3,4-^{3}H]glutamine, similar to ^{3}H-glutamine assay casein short. 0.05 kBq were added to each well with an incubation time of 30 minutes. The samples were prepared by pipetting 100 µL into 2 mL of scintillation cocktail and shaking overnight, then measured on a scintillation counter for 60 seconds each. For recovery reasons, a reference with the total initial activity was also measured.

4.3.4 Uptake assay in a MultiScreen® ("uptake assay II")

Cells were generally seeded in 75 cm^{2} sterile flasks 2 days before the experiment. Unspecific binding in the MultiScreen® wells was pre-blocked for 30 minutes with 100 µL of respective uptake medium per well. The cells cultivated in the flasks were scraped and counted. Cell suspensions were distributed to falcons, centrifuged at 1200 RPM at room temperature for 4 minutes and the cell pellets resuspended in respective uptake media, to give a cell concentration of 140 000 cells per 90 µL. 90 µL of the cell suspensions were pipetted into each well. "Blank" wells were prepared by adding 90 µL of medium without cells. The plate was incubated for 30 minutes at 37°C for settling of the cells. 60 µL of radioactivity (corresponding to approximately 24 kBq of 2-[^{18}F]FDG and [^{18}F]4-FGln or 0.2 kBq of [3,4-^{3}H]glutamine, in DPBS) were pipetted into the wells. The plate was incubated for 60 minutes at 37°C. Medium was removed by suction with a vacuum pump followed by two washing steps with 100 µL of DPBS until no further drying of the filters was observed. The filters with 2-[^{18}F]FDG and [^{18}F]4-FGln were then punched into gamma counter tubes, which were measured for 30 seconds each. Filters with [3,4-^{3}H]glutamine were transferred to tubes for measurement in the scintillation counter and covered with 2 mL of scintillation cocktail. The tubes were shaken overnight and measured in the scintillation counter for 60 seconds each. For all measurements 3 tubes with 60 µL of total activity added to the wells were measured as references and count as 100 % recovery.

4.3.5 Data evaluation

Data was evaluated on Microsoft Excel. Among the multiscreen uptake experiments 3 outliers were detected and were not considered in the evaluation. Data sets with high similarity that were to be compared were analysed with a t-Test to determine a significant difference (95% confidence interval). The % uptake was always normalized to 100.000 cells.

4.4 Establishing calibration curves for fluorine-18 and tritium measurements

Triplicates of 17 dilutions of 2-[^{18}F]FDG in DPBS with different activity concentrations were prepared, 1 mL of each sample was measured for 30 seconds. 14 dilutions were within the linear range of the gamma counter and the measurements were used for establishing the calibration curve after subtracting blank measurements.

Triplicates of 11 dilutions of [^{3}H]Gln in DPBS were prepared and 100 µL of each dilution in 2 mL of scintillation cocktail was measured for 60 seconds on the scintillation counter after shaking overnight in the dark. The blank was measured with 3 scintillation tubes with only scintillation cocktail and subtracted from the counts measured for the samples. The two lowest dilutions were in the range of the background and thus not included in the calibration curve.

5. Results

The nomenclature used in the report of the results is in accordance to the consensus by Coenen et al.[47] and the amendment by Herth et al.[48]

5.1 Radiosynthesis

5.1.1 Release efficiency of [^{18}F]fluoride from Chromafix® PS-HCO_3^- cartridge

Table 1: Release efficiency of [^{18}F]fluoride from Chromafix® PS-HCO_3^- cartridge using 0.18 mL $KHCO_3$ (8 mg/mL) in 1 mL 18-crown-6 in methanol (8 mg/mL)

Loaded activity [MBq]	Retained activity [MBq]	% Eluted (decay corrected)
88	10	89
305	38	88
278	22	92
106	14	87
103	13	87
116	22	80
107	12	90
101	9	91
95	6	94
	Average release efficiency	89 ± 4

5.1.2 Reaction temperature

Reaction temperatures were varied between 70, 80 and 90°C in the first syntheses. Radiochemical conversion (RCC) to the intermediate and resulting stereochemical purity of the final product for the different reaction temperatures are summarized in Table 2. The precursor used for establishing the first purification method and the reaction temperature was of the batch obtained from ABX advanced chemical compounds (Radeberg, Germany). As it resulted in the second highest RCC and best stereochemical purity, a reaction temperature of 80°C was applied in subsequent syntheses.

Table 2: summary of first syntheses on the ELIXYS module with varying reaction temperatures, RCC to the intermediate and stereochemical purity of the final product compared to the references. Unavailability of data is marked "N/A".

	Results of first syntheses			References		
	(n=3)	(n=1)	(n=1)	Qu et al. (2011)[40]	X. Zhang et al. (2016)[41]	Y. Zhang et al. (2019)[49]
Reaction T (°C)	70	80	90	70	70	90
RCC (%)	7 ± 2	11	14	20	N/A	N/A
Stereochemical purity (%)	83 ± 4	91	76	89	90 ± 5	>95

Table 3: RCC in small scale synthesis with precursor batch 1 obtained from ABX advanced chemical compounds and batch 2 obtained from Memorial Sloan Kettering Cancer Center

	Date	RCC (%)
Batch 1	day 1	85
	day 1	82
	+ 3 days	58
	+ 3 days	19
	+ 1 month	22
Batch 2	day 1	82
	+ 5 days	36
	+ 6 days	66
	+11 days	9
	+ 2 weeks	52
	+ 1 month	32

5.1.3 Establishment of purification methods

The previously reported[50] purification using semi-preparative HPLC with a reverse-phase column and an acetonitrile/water mobile phase has been adapted by including a gradient. After testing different ratios and gradients, eluting with 20-90 % acetonitrile over 30 minutes resulted in the best separation and recovery among the trials. Figure 4 shows a characteristic chromatogram from a synthesis with this purification method, with the intermediate being eluted after 22 minutes. RCC in this case was 11 %, and precursor of the first batch was used (ABX advanced chemical compounds, Radeberg, Germany).

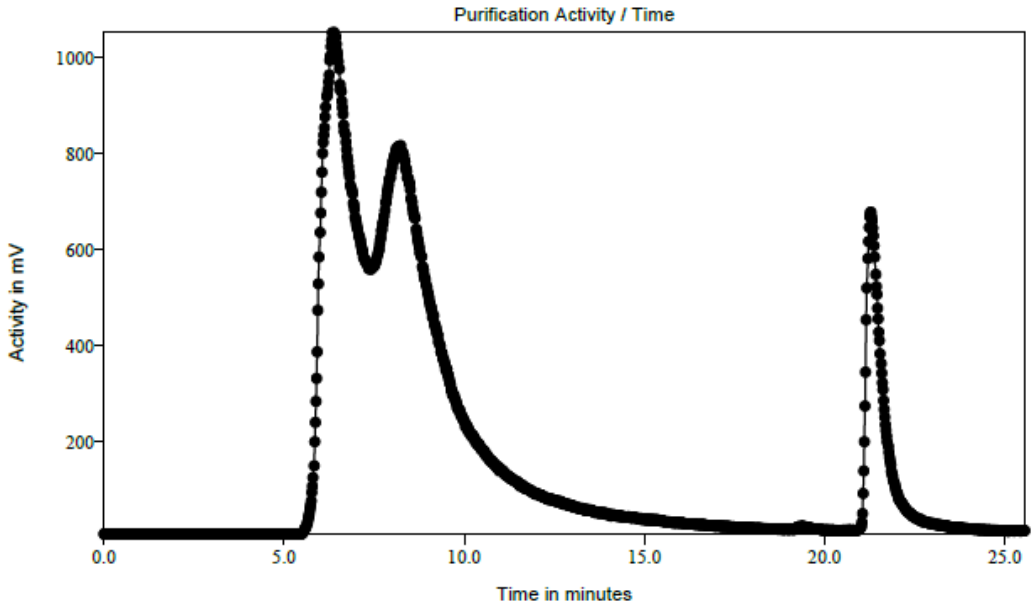

Figure 4: example chromatogram of a purification on a SUPERCOSIL ™LC-ABZ+ column, 20-90 % ACN/water (30 min), 5 mL/min flow, with intermediate peak at 22 minutes

The second semi-preparative purification method was adapted from the analytical HPLC method used to characterise the intermediate and from X. Zhang et al.[41] The intermediate is purified via a Gemini® C18 column, with methanol/water (8:2) + 0.1 % formic acid mobile phase and 5 mL/min flow. Figure 5 shows a corresponding chromatogram from the PURE/FORM unit, with the intermediate peak at 6.5 minutes. RCC was 93 % and the precursor used was from the second batch (Memorial Sloan Kettering Cancer Center, New York, USA).

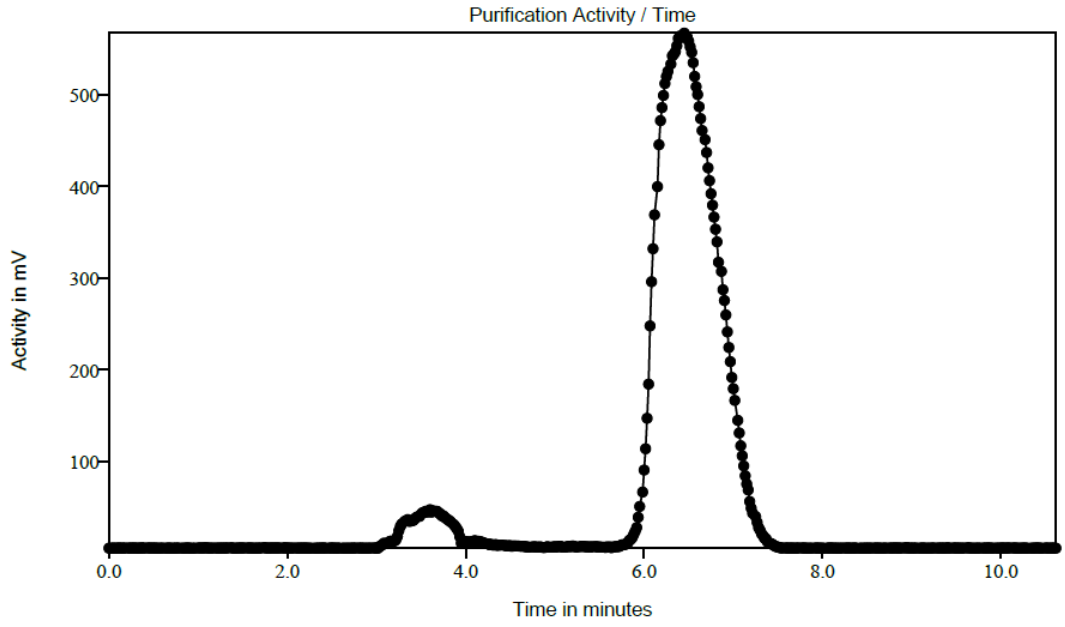

Figure 5: example chromatogram from an automated synthesis with on a Gemini® C18 column, methanol/water (8:2) + 0.1 % formic acid, 5 mL/min flow with intermediate peak at 6.5 minutes

The third and final purification method established does not include semi-preparative HPLC but is based on solid phase extraction (SPE). For this, four Oasis® HLB Light cartridges are conditioned, connected and mounted onto the PURE/FORM unit. Table 4 summarizes the results from the conducted automated synthesis using the three different purification methods in comparison to the references.

Table 4: Summary of synthesis parameters and results for all 3 established purification methods, in comparison to references. Unavailability of data is marked "N/A". "Precursor 1" and "Precursor 2" refer to the two different precursor batches.

		n=5	**n=59**	**n=5**	**n=2**	**n=5**
	Qu et al. (2011)[40]	**X. Zhang et al. (2016)**[41]	**Y. Zhang et al. (2019)**[49]	**Method 1 + precursor 1**	**Method 2 + precursor 2**	**Method 3 + precursor 2**
Reaction T (°C)	70	70	90	80	80	80
RCC (%)	20	N/A	N/A	8 ± 5	69; 93	78 ± 11
Purification method	SPE	Agilent XDB-C18, MeOH/water (7:3)	SPE	SUPER-COSIL® LC-ABZ+ ACN/water 20-90 % 30 min gradient	Gemini® C18, MeOH/ water (8:2)	SPE
t_R of interm. (min)		12 – 13		22	6 – 7	
Duration of synthesis (min)	N/A	80 ± 3	65 ± 5	115	100	100
RCY (%)	N/A (10 % non-corr.)	N/A (non-corr. 21 ± 3 %; according to synthesis duration 35 ± 3 %	18 ± 4	<8.3	no final product	20 ± 3
RCP (%)	99	>98	>90	91 ± 8	no final product	94 ± 5
Stereochem. purity (%)	89	90 ± 5	>95	82 ± 6	no final product	84 ± 6

5.1.4 Quality control

The analytical HPLC methods for characterizing intermediate and product were set up according to Qu et al.'s methods.[40] The RCC of the intermediate was determined on a Gemini® C18 column with methanol/water (8:2) + 0.1 % formic acid and a 1 mL/min flow rate. Free [^{18}F]fluoride eluted after around 2.5 min, the intermediate after approximately 6 min. A characteristic chromatogram is shown in Figure 6, derived from a synthesis with precursor from the second batch, with 88 % RCC.

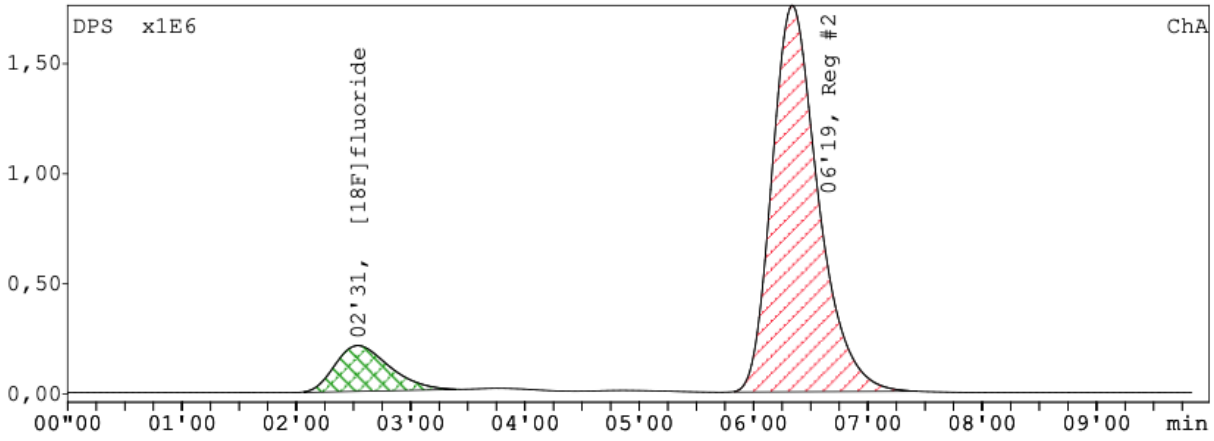

Figure 6: example chromatogram for determining RCC to intermediate (t_R=6'19), on a Gemini® C18 column, methanol/water (8:2) + 0.1 % formic acid, 1 mL/min flow

Radiochemical and stereochemical purity were determined with a chiral HPLC method, as seen in Figure 7. The product eluted after around 11 minutes, always confirmed by co-injecting non-radioactive standard 4-FGln. Radiochemical purity additionally had to be determined by the above-mentioned method, for recovery of residual intermediate. The product eluted after approximately 3 minutes. Free [^{18}F]fluoride can additionally be determined with the established TLC method, with which fluoride remains at the spotting line while the radiolabelled intermediate and product have higher R_f-values.

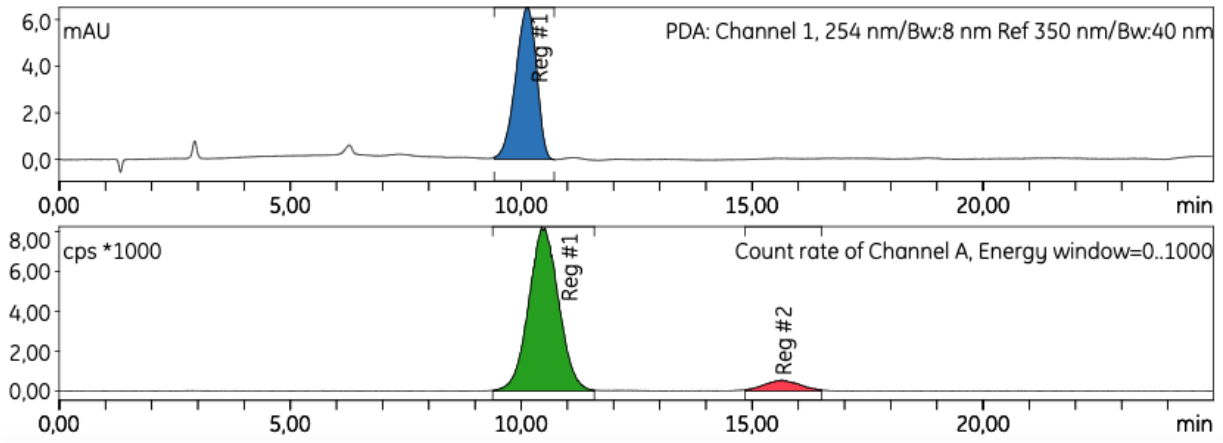

Figure 7: chromatogram of product [^{18}F]4-FGln spiked with non-radioactive standard 4-FGln, on a Phenomenex (D)-penicillamine column, 1mM $CuSO_4$, 1 mL/min flow, with product peak at 11 min.

5.2 Cell uptake assays

*Table 5: Summary of cell uptake assays. *Incubation time of 30 min, all others 60 min.*

	Uptake Assay I		**Uptake Assay II**	
	HT29	HT1080	HT29	HT1080
[3,4-^{3}H]Gln			*2.3 ± 0.2 % 5.8 ± 1.2 % (n=1)	*3.3 ± 0.7 % 7.8 ± 1.5 % (n=1)
2-[^{18}F]FDG	3.9 ± 0.6 % (n=3)	7.9 ± 3.7 % (n=3)	12.5 ± 3.3 % (n=5)	13.9 ± 4.7 % (n=5)
[3,4-^{3}H]Gln			2.1 ± 0.5 % (n=5)	4.0 ± 2.6 % (n=5)
[^{18}F]4-FGln			1.9 ± 0.9 % (n=4)	2.2 ± 0.8 % (n=3)

The results of the uptake assays are summarized in Table 5. Uptake in a 6-well-plate (further referred to as "uptake assay I") resulted in a significantly lower 2-[^{18}F]FDG uptake per 100.000 cells than the MultiScreen® method (further referred to as "uptake assays II") ($p < 0.001$). In addition, the difference in 2-[^{18}F]FDG uptake between the two cell lines was significant in uptake assays I, with a higher uptake in HT1080 cells ($p=0.005$), but not in the MultiScreen® method (Figure 9).

What can be derived from the uptake assays II, and was the case for both cell lines, was a higher uptake of 2-[^{18}F]FDG than of either of the glutamine derivatives. However, no significant difference was encountered between [^{18}F]4-FGln and [3,4-^{3}H]Gln uptake (Figure 8). For the two glutamine tracers a difference in avidity between the cell lines could also not be determined.

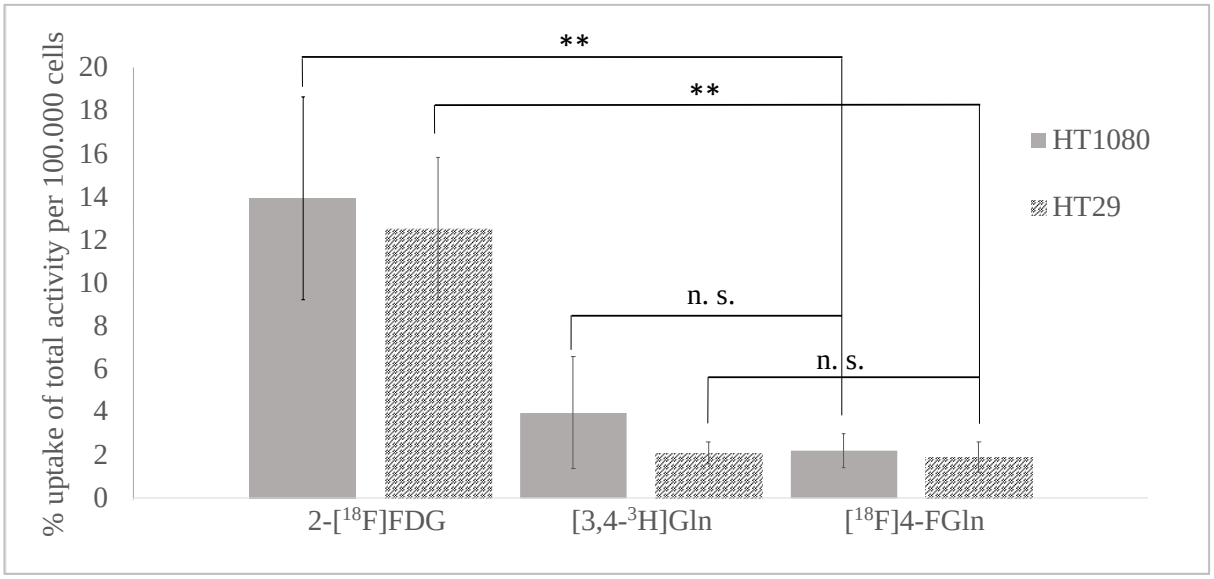

Figure 8: Average % uptake of 2-[^{18}F]FDG (n=5), [^{18}F]4-FGln (n=5) and [3,4-^{3}H]Gln (n=3 for HT1080, n=4 for HT29) per 100.000 HT29 and HT1080 Cells (uptake assay II)

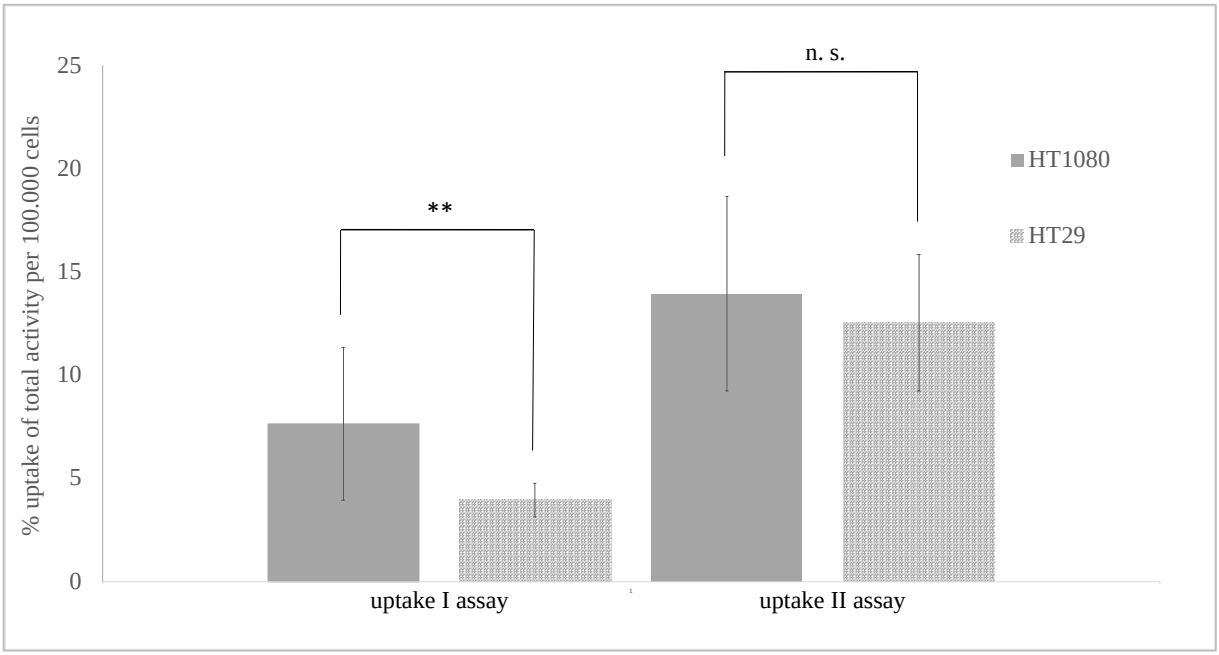

Figure 9: Comparison of average 2-[^{18}F]FDG uptake per 100.000 cells in HT1080 and HT29 cells determined with uptake assays I and II

6. Discussion

6.1 Radiosynthesis

6.1.1 Release efficiency of [^{18}F]fluoride from Chromafix PS-HCO_3^- cartridge

For the elution of [^{18}F]fluoride from the anion exchange cartridge, typically the base K_2CO_3 is used with the phase transfer catalyst Kryptofix® 222. However, it has been reported that the reaction is sensitive to basicity, and epimerization to all four stereoisomers is caused by this phase transfer catalyst. It has been shown that a much better optical purity of the product is ensured by replacement of these two agents by $KHCO_3$ and 18-crown-6, and additionally substituting the eluent acetonitrile with methanol. X. Zhang et al. reported a minimum of 95 % release efficiency of [^{18}F]fluoride with the alternative combination, which was not achieved within this work.[41] The values ranged from 87 to 94 %, with one lower exception (80 %). Indeed, it must be noted that these values were determined during the manual small-scale syntheses, and release efficiency in the automated syntheses on the module may deviate.[40,41]

6.1.2 Reaction temperature

Since a synthesis with 90°C reaction temperature yielded in product with lower stereochemical purity than previous syntheses with lower temperature (Table 2), a reaction temperature of 80°C was implemented for all subsequent syntheses. However, reacting at 80°C and 90°C was only tested once each on the ELIXYS with precursor from the batch obtained from ABX Advanced Chemical Compounds. Thus, to determine a correlation between temperature and stereoisomer formation, it would be necessary to repeat the synthesis under these conditions. Furthermore, Y. Zhang et al. reported much higher stereochemical purity (>95 %)[49], despite heating the reaction mixture at 90°C, yet they do not discuss the motivation behind or impact of using a significantly higher reaction temperature than what was reported in previous publications.

6.1.3 Establishment of the purification method

First, a purification method via semi-preparative HPLC on the ELIXYS was established, due to a reported improved radiochemical yield (by 20 %) by X. Zhang et al. in comparison with purification via SPE.[41] With the first purification method the intermediate peak eluted after 22 minutes. Generally, two to three further peaks appeared in the radio trace. A broad double peak eluted between approximately 6 and 10 minutes and a minor peak after around 19 minutes. One

major peak with a short retention time was expected due to unreacted [^{18}F]fluoride. The small peak eluting just before the intermediate may be structurally very similar to the latter, thus it might be a side product or partly hydrolysed intermediate. However, it was only a minor impurity (<1 %) and baseline separated from the intermediate.

On the ELIXYS synthesis module the reactor is an open vial that is closed off during adding and reacting steps, however there is no inert atmosphere maintained throughout the synthesis. Small scale manual syntheses were conducted to test whether an inert atmosphere positively impacts RCC of the precursor to the intermediate, and to attempt an alternative purification via solid phase extraction cartridges. Despite variation, higher RCC to the intermediate than in the previous automated syntheses (Table 2) and higher than was reported by Qu et al. (20 %)[40], was achieved in the manual runs (Table 3). This was suspected to be due to the decreased exposure of the reaction mixture to air compared to syntheses on the ELIXYS. However, when returning to automated synthesis for the establishment of the second semi-preparative HPLC purification method, the second precursor batch was used (Memorial Sloan Kettering Cancer Center, New York, USA) and more than 80 % conversion was then also achieved via automated synthesis (see Table 4). Thus, exposure to air during the synthesis could not have been the sole cause of the low conversion rates while establishing the first purification method. The second precursor batch had been stored at -80°C under inert gas, while the first precursor batch had been stored at only -20°C (as stated in the description received from the company). In addition, as can be seen in Table 3, RCC seemed to decrease after several syntheses had been conducted with precursor from the same aliquot from ABX. Synthesis with an aliquot of the second precursor batch also resulted in higher conversion in the first run, but this fluctuated over the following syntheses without a clear decreasing trend. Overall, stability of the precursor should be evaluated in the future but there are indications that it is significantly influenced by the storage conditions, which may explain the better RCC achieved with precursor of the second batch.

The second semi-preparative purification method was adapted from the analytical HPLC method implemented for determining the conversion rate of the precursor to the intermediate, so it was thought suitable for separation of the compounds on a semi-preparative HPLC column. In addition, this was done successfully by X. Zhang et al., who also used a semi-preparative HPLC method consisting of a C18 column and 73.5% MeOH, 26.5% water + 0.1 % formic acid and analytical HPLC of the intermediate with the analytical equivalent of the column and an almost identical mobile phase (75 % MeOH and 25% water, 0.1% formic acid).[41]

While radiochemical yields with the first purification method via semi-preparative HPLC were low (<3.8 %, non-decay corrected), the final yields in the syntheses with the second method using the second precursor batch could not be determined due to technical problems encountered with the PURE/FORM, to prove a higher final yield due to a significantly improved conversion rate (see Figure 4 and Figure 5 in comparison). Syntheses using the second precursor batch with the two semi-preparative HPLC purification methods would have to be repeated to compare the final yields with the improved conversion rate.

The SPE purification method was based on Qu et al. and Y. Zhang et al.'s reported methods[40,49], who used an Oasis® HLB 3cc Vac cartridge (sorbent mass was not stated). Due to unavailability of the reported cartridge, the Oasis® HLB Light cartridges were used instead, which possess the same chemical properties and are only shaped differently. None of the attempts in the manual small-scale syntheses were successful however, despite diluting the reaction mixture with up to 50 mL of water and using up to four consecutive cartridges to account for a higher sorbent mass in cartridges used in the references. It proved difficult to manually load such a large volume onto four consecutive cartridges, which is why a set up with N_2 was assembled, that loaded the cartridges with the diluted reaction mixture by blowing N_2 into a dilution flask and trapping the contents on the cartridges. This was an improvement in terms of practicality and radiation protection; however, trapping of the intermediate was still not efficient. Overall, manual syntheses were only successful up to conversion to the intermediate. The cartridge method was nevertheless set up on the ELIXYS. Indeed, it finally resulted in the most successful and reproducible syntheses of the three methods (Table 4) and was finally the method used to produce [^{18}F]4-FGln for the in vitro experiments. Radiochemical yield was 20 ± 3 % on average, which is comparable to Y. Zhang et al.'s reports[49]. Radiochemical and stereochemical purity could not quite match the purities reported in the references, with 94 ± 5 % and 84 ± 6 %, respectively.

The total synthesis time of the SPE method was equal to synthesis with the second semi-preparative HPLC method (~100 min), in which the intermediate is eluted approximately 15 minutes earlier than in the first semi-preparative purification method. Moreover, it could possibly be shortened further by adapting the formulation steps - such as decreasing the dilution volume or reviewing the necessity of the rinse step.

6.1.4 Quality control

To determine the purity of the produced (2S,4R)-[^{18}F]4-FGln, it must be noted that for radiochemical and stereochemical purity three methods have to be used: TLC for determination of free [^{18}F]fluoride, a chiral HPLC method for the stereochemical purity and RP-HPLC for residual [^{18}F]F-intermediate. In detail, to test whether only one HPLC system can be used to determine stereochemistry and unreacted intermediate, several tests were performed by injection of the radiolabelled intermediate and [^{18}F]fluoride. It seems that unconverted intermediate is not recovered by the chiral method, which is demonstrated by comparing Figure 7, Figure 10, Figure 11 Figure 12. Figure 10 is a chromatogram obtained after injecting the non-purified intermediate (69 % conversion), while Figure 11 shows a measurement of [^{18}F]fluoride with the same HPLC method. The shapes (extreme tailing) and retention times (5.57 and 5.68 min) of the two peaks are very similar, which leads to the assumption that Figure 10 only shows the unreacted [^{18}F]fluoride and the intermediate was actually not eluted. Figure 7 shows the chromatogram of a product with the chiral HPLC method, with the product peak at 10.5 minutes, and a peak at 16 minutes. Characterizing the product with this chromatogram leads to 100 % radiochemical purity (assuming that the peak at 16 minutes is due to a stereoisomer) and 93 % stereochemical purity. However, when injecting the same product onto the RP-HPLC used for characterizing the intermediate, the product peak (~3 min) is not the only peak (Figure 12). There are two more small peaks between 6 and 7 minutes, which corresponds to the retention time of the intermediate, resulting in only 84 % radiochemical purity. Thus, it has been shown that it is not sufficient to evaluate radiochemical purity with the chiral analytical HPLC method and the purities stated in the reference papers should be taken with caution.

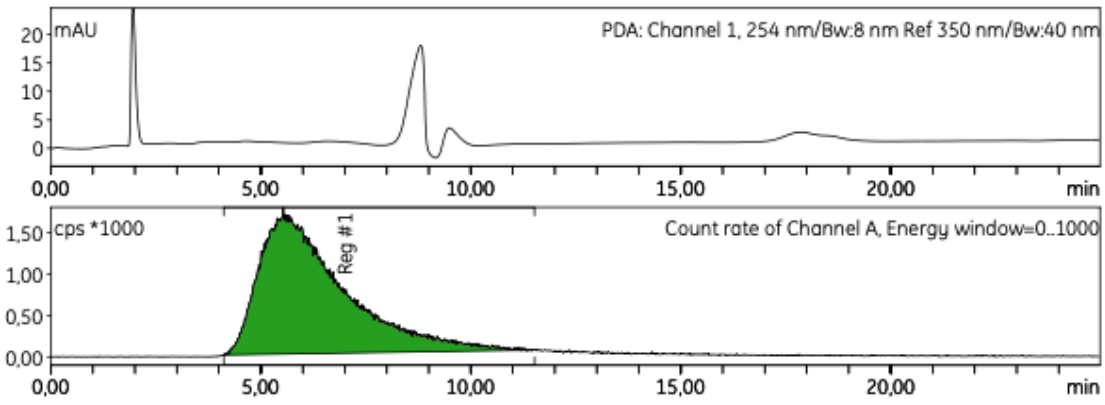

Figure 10: measurement of the not purified intermediate (69 %) with the chiral HPLC method. (t_R=5.57 min, extreme tailing)

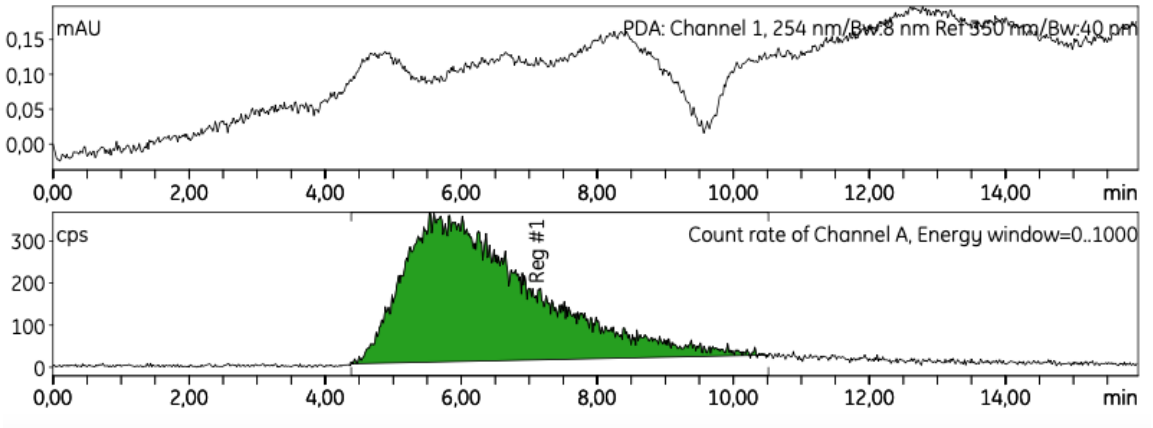

Figure 11: measurement of pure [^{18}F]fluoride with the chiral HPLC method (t_R=5.68 min, extreme tailing)

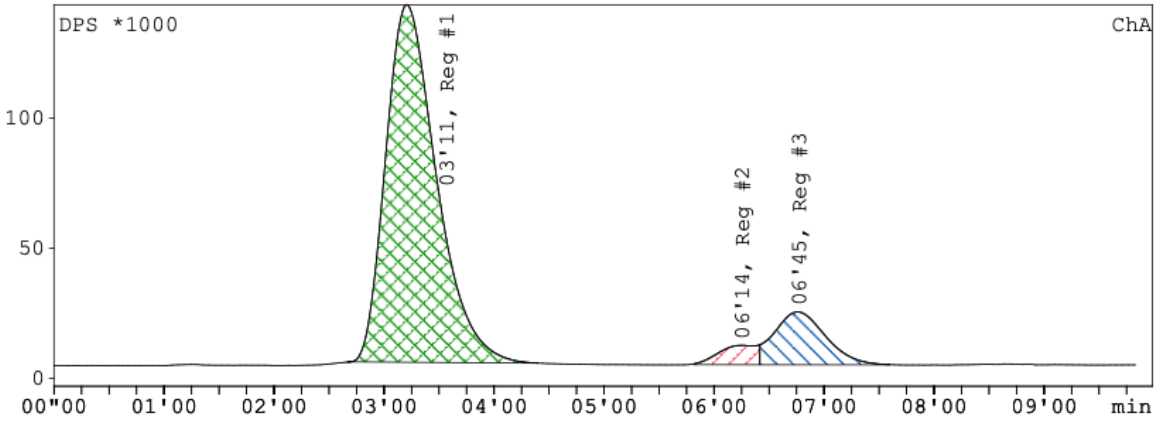

Figure 12: chromatogram of [^{18}F]4-FGln (region 1) on a Gemini® C18, methanol/water (8:2) + 0.1 % formic acid (8/2), 1 mL/min flow. Same product mixture as seen in Figure 7

Average radiochemical purity of the product over all successful automated syntheses was 93 ± 6 % (n=10), according to the chiral HPLC method. For synthesis with semi-preparative purification, it was 91 ± 8 % and with the SPE method 94 ± 5 %. A slightly better stereochemical purity was achieved in the syntheses with SPE purification than with the first purification method (see Table 4). Except for Y. Zhang et al.'s results, who reported radiochemical purities of >90 %, the references mostly stated significantly higher percentages (>97 %), determined with the same chiral HPLC method. Stereochemical purities published range from 85 % upwards, the highest reported by X. Zhang et al. and Lieberman et al. (98 % and 91 ± 8 %, respectively) and where thus also higher than those achieved in this work.[40–42,49] Based solely on the retention time, the peak at 16 minutes could not be identified as a specific stereoisomer, as a reference standard was not available, but this peak always appeared in the quality control, even in the case of a product with a single peak in the HPLC method of the intermediate which

would suggest 100 % radiochemical purity. Qu et al. reported the product (2S,4R) to have had a retention time of 11 min, the (2R,4S)-isomer eluting after 15 min and the (2R,4R)-isomer after 18 min[40]. While the retention time of the product aligns and was confirmed by co-injecting with non-radioactive standard 4-FGln with the same stereochemistry, it can only be assumed that the second peak represents the stereoisomer with inverted stereochemistry (2R,4S). Therefore, comparing with the reported retention profiles, the peak deriving from a stereoisomer is the most plausible explanation. Nevertheless, Y. Zhang et al. additionally reported the formation of [^{18}F]F-Glu (t_R ~22 min) by hydrolysis of the glutamine (t_R ~15 min)[49]. Both explanations need proof with reference standards.

High radio- and stereochemical purity are pivotal to ensure that the image obtained via PET is derived from that specific radiolabelled species and can be interpreted accordingly. For the commonly used PET-tracer 2-[^{18}F]FDG, the release criteria for in-human application according to the European Pharmacopoeia (9th edition) include a minimum radiochemical purity of 95 %, and maximum stereochemical impurity of 10 % in form of 2-[^{18}F]fluoro-2-deoxy-D-mannose.[51] The radiochemical purity was achieved in some [^{18}F]4-FGln syntheses, however it should be guaranteed and should in the future always be confirmed with the RP-HPLC method as discussed above. In terms of stereochemical purity of the final product there is also room for improvement. A higher and more rapid transport into the cell of the stereoisomers that are analogs of natural L-glutamine has been shown with in vitro experiments.[40] Thus it is not sufficient to synthesize a radiochemically pure [^{18}F]F-Gln, but high optical purity of at least the α-amino group is necessary for a successful transport of the radiotracer into the cells. While the maximum uptake in 9L tumour cells of the (2S,4S)-isomer after 60 minutes has been shown to be comparable to the (2S,4R)-isomer, the first exhibited faster kinetics and intracellular levels were much lower at later time points. In glutamine-addicted SF188bclxl tumour cells, the (2S,4R)-isomer reached a higher uptake within 30 minutes, but was lower after 60 minutes.[40] Thus, uptake and retention can be dependent on the stereochemistry and in the future the impurity eluting after around 16 minutes in the chiral HPLC method and the cause of its formation should be identified and diminished.

6.2 Cell uptake assays

6.2.1 Discussion of the results

A summary of the cell uptake results is found in Table 5. Uptake assays I demonstrated a higher FDG uptake in HT1080 than in HT29 cells. Comparing the uptake of the three radiotracers

using uptake assays II, 2-[^{18}F]FDG uptake was significantly higher than of the glutamine derivatives. Both cell lines showed no significant difference in uptake of [^{18}F]4-FGln and [3,4-^{3}H]Gln.

Since the cell lines are not known to exhibit glutamine addiction, but both depend on glucose[52,53], it was not expected that uptake of the synthesized product would be higher than that of 2-[^{18}F]FDG, however similar uptake rate to [^{18}F]4-FGln in the first 60 minutes has been reported in non-glutamine addicted 9L tumour cells by Qu et al.[40] Thus, the difference after incubation for 60 minutes could also have been less pronounced. In addition, they reported that the uptake rate of [3,4-^{3}H]Gln up to 60 minutes was lower compared to [^{18}F]4-FGln in both the glutamine addicted SF-188bclxl and non-glutamine addicted 9L tumour cell line.[40,42] In vitro uptake studies by Ploessl et al. have suggested that [^{18}F]4-FGln is transported into the cell mainly via the SCL1A5 transporter, the same as L-glutamine.[42] Thus, it would be interesting if the non-naturally occurring fluorinated analogion is taken up even more rapidly. Apart from its transport, according to enzymological studies by Cooper et al., metabolism of (2S,4R)-4-FGln involves some of the same enzymes as L-glutamine metabolism, with differences in the conversion rates. For example, they found that interestingly 4-FGln was a better substrate of the kidney isozyme of glutaminase (GLS1), which is expressed in most cancers. It seems the chemical properties of the fluorine atom can aid enzymatic transformation. However, it can also hinder it, as they showed in the case of synthetases, which did not convert 4-FGlu back to 4-FGln in their in vitro studies, which would be the case for the naturally occurring analogue.[54] The conversion rate by different glutamine aminotransferases was lower than for L-Gln[54]. In this case it would be expected that preferably [3,4-^{3}H]Gln is metabolised, as it is indistinguishable from glutamine.

Studies of protein incorporation of [^{18}F]4-FGln in 9L and SF-188bclxl cells increased up to 2 hours, with 72 and 62 %, respectively, and was similar to [3,4-^{3}H]Gln[42,55]. At the same time 4-FGlu is minimally incorporated into protein.[55] This is an interesting aspect, as [^{18}F]4-FGln derived [^{18}F]4-FGlu may be less built into protein than [3,4-^{3}H]Gln derived glutamate, and protein incorporation is relevant as a way of trapping of radioactivity in the cells. Conversion of 4-FGln to 4-FGlu via glutaminase and then to α-KG by alanine aminotransferase has been demonstrated in vivo, which generates free fluoride.[54] Via in vivo metabolism studies Lieberman et al. found that, within their experimental conditions, activity that was not trapped within tumour in vivo was mainly ascribed to [^{18}F]4-FGln (70-80 % approximately), and small fractions each (around 8-9 %) were due to the metabolites [^{18}F]4-FGlu and free [^{18}F]fluoride, one hour after injection.[42] It is unclear however, whether [^{18}F]fluoride was derived from efflux

from the cells, or from defluorination of the radiotracer in the plasma. Efflux of glutamine is regulated in part by extracellular concentrations of other amino acids through shared membrane antiporters.[46] 2-[^{18}F]FDG is transported into the cell by glucose transporters, followed by a rapid phosphorylation by hexokinase. In this form it is metabolized and cleared from the cells slowly.[56,57]

Overall, the results of the uptake assays comparing the radiotracers are not surprising, due to similar metabolism of the two glutamine tracers, known glucose avidity of the two tumour cell lines, and metabolic trapping of 2-[^{18}F]FDG in tumour cells. It is however difficult to compare the results to available in vitro data, as the radiotracer kinetics and metabolic patterns certainly differ between tumour cell lines and there was no data found specifically for the two cell lines used in this work. Even then, uptake may vary between experiments due to factors such as incubation time, proliferative index of the cells, cell starving prior to uptake, activity, and use of different incubation media.[58,59]

6.2.2 Discussion and comparison of the experimental methods

The first uptake experiments were conducted in 6-well-plates with 2-[^{18}F]FDG only. The remaining experiments were conducted with a MultiScreen® system allowing a high throughput of experiments. Before availability of the [^{18}F]4-FGln PET-tracer, a pre-experiment was conducted (via uptake assay II) with [3,4-^{3}H]Gln using different incubation times to determine if a sufficient cell uptake is reached at 30 minutes, as the in vivo pharmacokinetics by Grkovski et al. showed a highest standardized uptake value after 30 minutes in 70 % of lesions they evaluated.[60] In this work it was found, that [3,4-^{3}H]Gln uptake increased until at least 60 minutes of incubation (Table 5). Therefore, an incubation time of 60 minutes was implemented for the subsequent experiments in order to compare all three radiotracers.

The cell numbers per well that were seeded varied due to different extents of cell death while scrapping. To ensure enough repeats, in one uptake assay II the cell number per well of the HT29 cell line was only 75.000, which was markedly lower than in the other experiments, and this resulted in the highest 2-[^{18}F]FDG and [3,4-^{3}H]Gln uptake (28.0% and 8.9%, respectively, vs. the average % uptake listed in Table 5). Similarly, for the HT1080 cell line, in one experiment the cell number per well was 87.000, which resulted in the highest 2-[^{18}F]FDG and [^{18}F]4-FGln uptake of all experiments (25.8% and 3.8%, respectively vs. average % uptake listed in Table 5). In order to minimize the influence of high cell number variation on the results, only the results from experiments with 110.000-140.000 cells per well were used in the

calculation of the average uptake values. In the future, testing of the cell number should be performed.

The differences in results among uptake assays I and II show that the experimental set up highly influences the outcome. Naturally the question arises, which experiment is more suitable. The coefficient of variation (CV) (of multiplicate of same experimental condition) in uptake assays I ranged from 1 to 20 % with an average of 7 ± 6 % (n=6), while in uptake assays II they ranged from 2 to 44 with an average of 16 ± 8 % (n=32). Lower variation coefficients indicate that the results obtained with uptake assays I were more reproducible than those obtained with the MultiScreen® method. While conducting the experiments several sources of errors or inconsistencies, as well as advantages and disadvantages of both experimental methods became obvious and shall be discussed here.

The experimental setup using the MultiScreen® is particularly appealing due to the possibility to conduct high throughput experiments. Within one experiment, just one well-plate, several different conditions can be tested and compared, while ensuring a sufficiently high number of replicas in a shorter time. The 96-well-MultiScreen® plates allow for the use of multichannel pipettes which reduces the pipetting workload compared to what would be necessary to achieve the same throughput with the regular well plates.

The first step with uptake assay II was the pre-wetting of the filters with medium. In some cases, it was observed that the plate, which has tiny openings under each well for the later removal of medium with the vacuum pump, leaked in some areas. After the first couple experiments it was properly checked already during the pre-wetting whether all wells were leakproof. It might falsify the results, if uptake medium with activity is lost during incubation and not available for cell uptake. This is one possible cause for high variation among the wells.

As mentioned, in the results of two experiments via uptake assay II, it was visible that the cell number had a significant impact on the uptake. On the one hand, using less than 100.000 cells per well resulted in a higher uptake, on the other hand, a high cell number might lead to blocking of the filters, or to multi-layer formation and subsequently reduced uptake in the lower cell layers. Using the 6-well-plate uptake experiments, the cell number has to be determined within the experiments as well. However, microscopy is possible and therefore determining the actual transferred, attached, and viable cells in comparison to the MultiScreen®. In the uptake assay II, there is a higher DPBS amount when incubating. In a pre-experiment it was found that cells fully detached when incubated in pure DPBS, which in this case was not an issue as cells were not required to be fully attached to the wells for the uptake. However overall nutrient

concentration from the medium is lower. In addition, as in the smaller wells of the 96-well-multiscreen the dilution of the radiotracers made up 40 % of the total volume, and pipetting this volume onto the cell suspensions surely leads to higher activity concentration than in the uptake assays I. This could be a possible explanation for a higher 2-[^{18}F]FDG uptake in the assays using a MultiScreen® compared to uptake assays I.

Higher uptake values in uptake assays II than in the uptake assays I might also be due to inefficient drying of the filters which may falsify the cell uptake values. In some cases, medium was not removed equally from the wells, and the filters were still moist. However, remaining activity that should be counted to the supernatant fraction should not have such a big impact, as the filters were washed twice with DPBS, so in the remaining moisture on the filters there should ideally only be traces of radioactivity left. CV was even much more pronounced in the case of the blank wells however, with an average of 45 % (± 21 %). In the uptake I experiments the supernatant is removed with a pipette from the wells, and they are washed, but still there may always a small amount of activity not accounted for in the supernatant and added to the cell fraction.

In the uptake I experiments the issue was encountered that when measuring [3,4-^{3}H]Gln in the gamma counter, 200 µL of the total cell suspension was measured in 2 mL of scintillation cocktail, however the cells tended to clump together after sitting for some time and it was difficult to resuspend them. Those measurements were not used in the end due to insufficient initial activity for measurements on the scintillation counter. However, it is a noteworthy practical advantage of the uptake assays II, that the total amount of cells (on the filter) is measured in the scintillation counter, and no further pipetting is necessary.

To summarize, the MultiScreen® method has a lot of potential for high throughput experiments, and after a few repeats and experience with the handling, the potential sources of errors could increasingly be prevented or evened out.

7. Conclusion

In the course of this work, the automated synthesis of (2S,4R)-[^{18}F]4-fluoroglutamine on a FLEX/CHEM automated synthesizer (SOFIE Biosciences, USA) for potential application as a PET-tracer was successfully set up. Three methods of purification of the radiolabelled intermediate were established, two using semi-preparative HPLC and one employing SPE cartridges, whereas the latter showed the most promising results. Furthermore, methods for the

quality control of the intermediate (RP-HPLC) and the final product (chiral HPLC) were implemented. With the SPE method the average RCY of the product was 20 ± 3 % (n=5) and the RCP was 94 ± 5 %, both of which are comparable to Y. Zhang et al.'s reported results. The average stereochemical purity of 84 ± 6 % was lower than in previous reports and can therefore be further improved. It was shown that RCP of the product should additionally be validated with the RP-HPLC method in order to determine residual intermediate. Uptake of the radiotracer in HT29 and HT1080 cells was approximately 2 % of the total activity per 100.000 cells for both cell lines, which was similar to [3,4-^{3}H]Gln, but significantly lower than 2-[^{18}F]FDG uptake. Therefore, it must be further evaluated whether (2S,4R)-[^{18}F]4-FGln is a candidate for cancer diagnosis and also whether it is superior to 2-[^{18}F]FDG in terms of selectivity of tumour cell versus immune cell uptake.

References

(1) Altman, B. J.; Stine, Z. E.; Dang, C. V. From Krebs to Clinic: Glutamine Metabolism to Cancer Therapy. *Nat. Rev. Cancer* **2016**, *16* (10), 619–634. https://doi.org/10.1038/nrc.2016.71.

(2) Croteau, E.; Renaud, J. M.; Richard, M. A.; Ruddy, T. D.; Bénard, F.; deKemp, R. A. PET Metabolic Biomarkers for Cancer: Supplementary Issue: Biomarkers and Their Essential Role in the Development of Personalised Therapies (A). *Biomark. Cancer* **2016**, *8s2*, BIC.S27483. https://doi.org/10.4137/BIC.S27483.

(3) Long, N. M.; Smith, C. S. Causes and Imaging Features of False Positives and False Negatives on 18F-PET/CT in Oncologic Imaging. *Insights Imaging* **2011**, *2* (6), 679–698. https://doi.org/10.1007/s13244-010-0062-3.

(4) Pavlova, N. N.; Thompson, C. B. The Emerging Hallmarks of Cancer Metabolism. *Cell Metab.* **2016**, *23* (1), 27–47. https://doi.org/10.1016/j.cmet.2015.12.006.

(5) Vaupel, P.; Multhoff, G. Revisiting the Warburg Effect: Historical Dogma *versus* Current Understanding. *J. Physiol.* **2021**, *599* (6), 1745–1757. https://doi.org/10.1113/JP278810.

(6) Choi, Y.-K.; Park, K.-G. Targeting Glutamine Metabolism for Cancer Treatment. *Biomol. Ther.* **2018**, *26* (1), 19–28. https://doi.org/10.4062/biomolther.2017.178.

(7) Momcilovic, M.; Shackelford, D. B. Imaging Cancer Metabolism. *Biomol. Ther.* **2018**, *26* (1), 81–92. https://doi.org/10.4062/biomolther.2017.220.

(8) Chen, L.; Cui, H. Targeting Glutamine Induces Apoptosis: A Cancer Therapy Approach. *Int. J. Mol. Sci.* **2015**, *16* (9), 22830–22855. https://doi.org/10.3390/ijms160922830.

(9) Yoo, H. C.; Yu, Y. C.; Sung, Y.; Han, J. M. Glutamine Reliance in Cell Metabolism. *Exp. Mol. Med.* **2020**, *52* (9), 1496–1516. https://doi.org/10.1038/s12276-020-00504-8.

(10) Abdel-Wahab, A. F.; Mahmoud, W.; Al-Harizy, R. M. Targeting Glucose Metabolism to Suppress Cancer Progression: Prospective of Anti-Glycolytic Cancer Therapy. *Pharmacol. Res.* **2019**, *150*, 104511. https://doi.org/10.1016/j.phrs.2019.104511.

(11) Carlson, S. A Glance At The History Of Nuclear Medicine. *Acta Oncol.* **1995**, *34* (8), 1095–1102. https://doi.org/10.3109/02841869509127236.

(12) Yeong, C.-H.; Cheng, M.; Ng, K.-H. Therapeutic Radionuclides in Nuclear Medicine: Current and Future Prospects. *J. Zhejiang Univ. Sci. B* **2014**, *15* (10), 845–863. https://doi.org/10.1631/jzus.B1400131.

(13) Kratz, J.-V.; Lieser, K. H. *Nuclear and Radiochemistry - Fundamentals and Applications.* Wiley-VCH: Weinheim, 2013.

(14) Wadsak, W.; Mitterhauser, M. Basics and Principles of Radiopharmaceuticals for PET/CT. *Eur. J. Radiol.* **2010**, *73* (3), 461–469. https://doi.org/10.1016/j.ejrad.2009.12.022.

(15) Edelmann, M. R. Radiolabelling Small and Biomolecules for Tracking and Monitoring. *RSC Adv.* **2022**, *12* (50), 32383–32400. https://doi.org/10.1039/D2RA06236D.

(16) Maddahi, J.; Packard, R. R. S. Cardiac PET Perfusion Tracers: Current Status and Future Directions. *Semin. Nucl. Med.* **2014**, *44* (5), 333–343. https://doi.org/10.1053/j.semnuclmed.2014.06.011.

(17) Van De Watering, F. C. J.; Rijpkema, M.; Perk, L.; Brinkmann, U.; Oyen, W. J. G.; Boerman, O. C. Zirconium-89 Labeled Antibodies: A New Tool for Molecular Imaging in Cancer Patients.

BioMed Res. Int. **2014**, *2014*, 1–13. https://doi.org/10.1155/2014/203601.

(18) Baum, R. P.; Kulkarni, H. R. THERANOSTICS: From Molecular Imaging Using Ga-68 Labeled Tracers and PET/CT to Personalized Radionuclide Therapy - The Bad Berka Experience. *Theranostics* **2012**, *2* (5), 437–447. https://doi.org/10.7150/thno.3645.

(19) Zalutsky, M.; Vaidyanathan, G. Astatine-211-Labeled Radiotherapeutics An Emerging Approach to Targeted Alpha-Particle Radiotherapy. *Curr. Pharm. Des.* **2000**, *6* (14), 1433–1455. https://doi.org/10.2174/1381612003399275.

(20) Banerjee, S. R.; Pomper, M. G. Clinical Applications of Gallium-68. *Appl. Radiat. Isot.* **2013**, *76*, 2–13. https://doi.org/10.1016/j.apradiso.2013.01.039.

(21) Petroni, D.; Menichetti, L.; Poli, M. Historical and Radiopharmaceutical Relevance of [18F]FDG. *J. Radioanal. Nucl. Chem.* **2020**, *323* (3), 1017–1031. https://doi.org/10.1007/s10967-020-07013-y.

(22) Petriev, V. M.; Tishchenko, V. K.; Krasikova, R. N. 18F-FDG and Other Labeled Glucose Derivatives for Use in Radionuclide Diagnosis of Oncological Diseases (Review). *Pharm. Chem. J.* **2016**, *50* (4), 209–220. https://doi.org/10.1007/s11094-016-1425-y.

(23) Hess, S.; Blomberg, B. A.; Zhu, H. J.; Høilund-Carlsen, P. F.; Alavi, A. The Pivotal Role of FDG-PET/CT in Modern Medicine. *Acad. Radiol.* **2014**, *21* (2), 232–249. https://doi.org/10.1016/j.acra.2013.11.002.

(24) Klebermass, E.-M.; Mahmudi, M.; Geist, B. K.; Pichler, V.; Vraka, C.; Balber, T.; Miller, A.; Haschemi, A.; Viernstein, H.; Rohr-Udilova, N.; Hacker, M.; Mitterhauser, M. If It Works, Don't Touch It? A Cell-Based Approach to Studying 2-[18F]FDG Metabolism. *Pharmaceuticals* **2021**, *14* (9), 910. https://doi.org/10.3390/ph14090910.

(25) Abouzied, M. M.; Crawford, E. S.; Nabi, H. A. 18F-FDG Imaging: Pitfalls and Artifacts. *J. Nucl. Med. Technol.* **2005**, *33* (3).

(26) Venneti, S.; Dunphy, M. P.; Zhang, H.; Pitter, K. L.; Zanzonico, P.; Campos, C.; Carlin, S. D.; La Rocca, G.; Lyashchenko, S.; Ploessl, K.; Rohle, D.; Omuro, A. M.; Cross, J. R.; Brennan, C. W.; Weber, W. A.; Holland, E. C.; Mellinghoff, I. K.; Kung, H. F.; Lewis, J. S.; Thompson, C. B. Glutamine-Based PET Imaging Facilitates Enhanced Metabolic Evaluation of Gliomas in Vivo. *Sci. Transl. Med.* **2015**, *7* (274). https://doi.org/10.1126/scitranslmed.aaa1009.

(27) Vaidyanathan, S.; Patel, C. N.; Scarsbrook, A. F.; Chowdhury, F. U. FDG PET/CT in Infection and Inflammation—Current and Emerging Clinical Applications. *Clin. Radiol.* **2015**, *70* (7), 787–800. https://doi.org/10.1016/j.crad.2015.03.010.

(28) Cheson, B. D. Rethinking Clinical Response and Outcome Assessment in a Biologic Age. *Curr. Oncol. Rep.* **2015**, *17* (6), 27. https://doi.org/10.1007/s11912-015-0452-2.

(29) Al-Ibraheem, A.; Abdlkadir, A. S.; Juweid, M. E.; Al-Rabi, K.; Ma'koseh, M.; Abdel-Razeq, H.; Mansour, A. FDG-PET/CT in the Monitoring of Lymphoma Immunotherapy Response: Current Status and Future Prospects. *Cancers* **2023**, *15* (4), 1063. https://doi.org/10.3390/cancers15041063.

(30) Bader, J. E.; Voss, K.; Rathmell, J. C. Targeting Metabolism to Improve the Tumor Microenvironment for Cancer Immunotherapy. *Mol. Cell* **2020**, *78* (6), 1019–1033. https://doi.org/10.1016/j.molcel.2020.05.034.

(31) Reinfeld, B.; Madden, M.; Wolf, M.; Chytil, A.; Bader, J.; Patterson, A.; Cohen, A.; Ali, A.; Do, B.; Muir, A.; Lewis, C.; Hongo, R.; Young, K.; Brown, R.; Todd, V.; Huffstater, T.; Abraham, A.; O'Neil, R.; Wilson, M.; Xin, F.; Tantawy, M.; Merryman, W.; Johnson, R.; Williams, C.; Mason, E.; Mason, F.; Beckermann, K.; Vander Heiden, M.; Manning, H.; Rathmell, J.; Rathmell, W. *Cell*

Programmed Nutrient Partitioning in the Tumor Microenvironment; preprint; Cancer Biology, 2020. https://doi.org/10.1101/2020.08.10.238428.

(32) Paidisetty, S.; Blodgett, T. M. Brown Fat: Atypical Locations and Appearances Encountered in PET/CT. *Am. J. Roentgenol.* **2009**, *193* (2), 359–366. https://doi.org/10.2214/AJR.08.2081.

(33) Seo, Y.; Craig, M. C.; Murphy, S. T.; Feng, J.; Chen, X.; Yuneva, M. [18F]-(2S,4R)4-Fluoroglutamine PET Imaging of Glutamine Metabolism in Murine Models of Hepatocellular Carcinoma (HCC). *Mol. Imaging* **2022**, *2022*, 1–8. https://doi.org/10.1155/2022/5185951.

(34) Obara-Michlewska, M.; Szeliga, M. Targeting Glutamine Addiction in Gliomas. *Cancers* **2020**, *12* (2), 310. https://doi.org/10.3390/cancers12020310.

(35) Fogal, V.; Babic, I.; Chao, Y.; Pastorino, S.; Mukthavaram, R.; Jiang, P.; Cho, Y.-J.; Pingle, S. C.; Crawford, J. R.; Piccioni, D. E.; Kesari, S. Mitochondrial P32 Is Upregulated in Myc Expressing Brain Cancers and Mediates Glutamine Addiction. *Oncotarget* **2015**, *6* (2), 1157–1170. https://doi.org/10.18632/oncotarget.2708.

(36) Yoo, H. C.; Yu, Y. C.; Sung, Y.; Han, J. M. Glutamine Reliance in Cell Metabolism. *Exp. Mol. Med.* **2020**, *52* (9), 1496–1516. https://doi.org/10.1038/s12276-020-00504-8.

(37) Wise, D. R.; Thompson, C. B. Glutamine Addiction: A New Therapeutic Target in Cancer. *Trends Biochem. Sci.* **2010**, *35* (8), 427–433. https://doi.org/10.1016/j.tibs.2010.05.003.

(38) Poole, C. J.; Van Riggelen, J. MYC—Master Regulator of the Cancer Epigenome and Transcriptome. *Genes* **2017**, *8* (5), 142. https://doi.org/10.3390/genes8050142.

(39) Yoo, H. C.; Park, S. J.; Nam, M.; Kang, J.; Kim, K.; Yeo, J. H.; Kim, J.-K.; Heo, Y.; Lee, H. S.; Lee, M. Y.; Lee, C. W.; Kang, J. S.; Kim, Y.-H.; Lee, J.; Choi, J.; Hwang, G.-S.; Bang, S.; Han, J. M. A Variant of SLC1A5 Is a Mitochondrial Glutamine Transporter for Metabolic Reprogramming in Cancer Cells. *Cell Metab.* **2020**, *31* (2), 267-283.e12. https://doi.org/10.1016/j.cmet.2019.11.020.

(40) Qu, W.; Zha, Z.; Ploessl, K.; Lieberman, B. P.; Zhu, L.; Wise, D. R.; B. Thompson, C.; Kung, H. F. Synthesis of Optically Pure 4-Fluoro-Glutamines as Potential Metabolic Imaging Agents for Tumors. *J. Am. Chem. Soc.* **2011**, *133* (4), 1122–1133. https://doi.org/10.1021/ja109203d.

(41) Zhang, X.; Basuli, F.; Shi, Z.-D.; Xu, B.; Blackman, B.; Choyke, P. L.; Swenson, R. E. Automated Synthesis of [18F](2S,4R)-4-Fluoroglutamine on a GE TRACERlab™ FX-N Pro Module. *Appl. Radiat. Isot.* **2016**, *112*, 110–114. https://doi.org/10.1016/j.apradiso.2016.02.016.

(42) Lieberman, B. P.; Ploessl, K.; Wang, L.; Qu, W.; Zha, Z.; Wise, D. R.; Chodosh, L. A.; Belka, G.; Thompson, C. B.; Kung, H. F. PET Imaging of Glutaminolysis in Tumors by ^{18}F-(*2S,4R*)4-Fluoroglutamine. *J. Nucl. Med.* **2011**, *52* (12), 1947–1955. https://doi.org/10.2967/jnumed.111.093815.

(43) Li, C.; Huang, S.; Guo, J.; Wang, C.; Huang, Z.; Huang, R.; Liu, L.; Liang, S.; Wang, H. Metabolic Evaluation of MYCN-Amplified Neuroblastoma by 4-[18F]FGln PET Imaging. *Mol. Imaging Biol.* **2019**, *21* (6), 1117–1126. https://doi.org/10.1007/s11307-019-01330-9.

(44) Valtorta, S.; Toscani, D.; Chiu, M.; Sartori, A.; Coliva, A.; Brevi, A.; Taurino, G.; Grioni, M.; Ruffini, L.; Vacondio, F.; Zanardi, F.; Bellone, M.; Moresco, R. M.; Bussolati, O.; Giuliani, N. [18F](2S,4R)-4-Fluoroglutamine as a New Positron Emission Tomography Tracer in Myeloma. *Front. Oncol.* **2021**, *11*, 760732. https://doi.org/10.3389/fonc.2021.760732.

(45) Muthukumar, S.; Darden, J.; Crowley, J.; Witcher, M.; Kiser, J. A Comparison of PET Tracers in Recurrent High-Grade Gliomas: A Systematic Review. *Int. J. Mol. Sci.* **2022**, *24* (1), 408. https://doi.org/10.3390/ijms24010408.

(46) Dunphy, M. P. S.; Harding, J. J.; Venneti, S.; Zhang, H.; Burnazi, E. M.; Bromberg, J.; Omuro, A. M.; Hsieh, J. J.; Mellinghoff, I. K.; Staton, K.; Pressl, C.; Beattie, B. J.; Zanzonico, P. B.; Gerecitano, J. F.; Kelsen, D. P.; Weber, W.; Lyashchenko, S. K.; Kung, H. F.; Lewis, J. S. In Vivo PET Assay of Tumor Glutamine Flux and Metabolism: In-Human Trial of ^{18}F-(2*S*,4*R*)-4-Fluoroglutamine. *Radiology* **2018**, *287* (2), 667–675. https://doi.org/10.1148/radiol.2017162610.

(47) Coenen, H. H.; Gee, A. D.; Adam, M.; Antoni, G.; Cutler, C. S.; Fujibayashi, Y.; Jeong, J. M.; Mach, R. H.; Mindt, T. L.; Pike, V. W.; Windhorst, A. D. Consensus Nomenclature Rules for Radiopharmaceutical Chemistry — Setting the Record Straight. *Nucl. Med. Biol.* **2017**, *55*, v–xi. https://doi.org/10.1016/j.nucmedbio.2017.09.004.

(48) Herth, M. M.; Ametamey, S.; Antuganov, D.; Bauman, A.; Berndt, M.; Brooks, A. F.; Bormans, G.; Choe, Y. S.; Gillings, N.; Häfeli, U. O.; James, M. L.; Kopka, K.; Kramer, V.; Krasikova, R.; Madsen, J.; Mu, L.; Neumaier, B.; Piel, M.; Rösch, F.; Ross, T.; Schibli, R.; Scott, P. J. H.; Shalgunov, V.; Vasdev, N.; Wadsak, W.; Zeglis, B. M. On the Consensus Nomenclature Rules for Radiopharmaceutical Chemistry – Reconsideration of Radiochemical Conversion. *Nucl. Med. Biol.* **2021**, *93*, 19–21. https://doi.org/10.1016/j.nucmedbio.2020.11.003.

(49) Zhang, Y.; Zhang, L.; Yang, J.; Wu, Z.; Ploessl, K.; Zha, Z.; Liu, F.; Xu, X.; Zhu, H.; Yang, Z.; Zhu, L.; Kung, H. F. Initial Experience in Synthesis of (2*S*,4*R*)-4-[^{18}F]Fluoroglutamine for Clinical Application. *J. Label. Compd. Radiopharm.* **2019**, *62* (5), 209–214. https://doi.org/10.1002/jlcr.3719.

(50) Li, S.; Schmitz, A.; Lee, H.; Mach, R. H. Automation of the Radiosynthesis of Six Different 18F-Labeled Radiotracers on the AllinOne. *EJNMMI Radiopharm. Chem.* **2017**, *1* (1), 15. https://doi.org/10.1186/s41181-016-0018-0.

(51) Fludeoxyglucose [18F] injection. European Pharmacopoeia. 9 edition. Strasbourg, France: European Directorate for the Quality of the Medicines , 2016:1135-1137.

(52) Romero-Arias, A. C.; Sequeda-Castañeda, L. G.; Aristizábal-Pachón, A. F.; Morales, L. Effect of 6-Shogaol on the Glucose Uptake and Survival of HT1080 Fibrosarcoma Cells. *Pharmaceuticals* **2019**, *12* (3), 131. https://doi.org/10.3390/ph12030131.

(53) Martínez-Maqueda, D.; Miralles, B.; Recio, I. HT29 Cell Line. In *The Impact of Food Bioactives on Health*; Verhoeckx, K., Cotter, P., López-Expósito, I., Kleiveland, C., Lea, T., Mackie, A., Requena, T., Swiatecka, D., Wichers, H., Eds.; Springer International Publishing: Cham, 2015; pp 113–124. https://doi.org/10.1007/978-3-319-16104-4_11.

(54) Cooper, A. J. L.; Krasnikov, B. F.; Pinto, J. T.; Kung, H. F.; Li, J.; Ploessl, K. Comparative Enzymology of (2S,4R)4-Fluoroglutamine and (2S,4R)4-Fluoroglutamate. *Comp. Biochem. Physiol. B Biochem. Mol. Biol.* **2012**, *163* (1), 108–120. https://doi.org/10.1016/j.cbpb.2012.05.010.

(55) Ploessl, K.; Wang, L.; Lieberman, B. P.; Qu, W.; Kung, H. F. Comparative Evaluation of ^{18}F-Labeled Glutamic Acid and Glutamine as Tumor Metabolic Imaging Agents. *J. Nucl. Med.* **2012**, *53* (10), 1616–1624. https://doi.org/10.2967/jnumed.111.101279.

(56) Som, P.; Atkins, H. L.; Bandoypadhyay, D.; Fowler, J. S.; MacGregor, A. R.; Matsui, K.; Oster, Z. H.; Sacker, D. F. A FluorinatedGlucose Analog, 2-Fluoro-2-Deoxy-D-Glucose(F-18): Nontoxic Tracer for RapidTumor Detection. *21* (7).

(57) Zhu, A.; Lee, D.; Shim, H. Metabolic Positron Emission Tomography Imaging in Cancer Detection and Therapy Response. *Semin. Oncol.* **2011**, *38* (1), 55–69. https://doi.org/10.1053/j.seminoncol.2010.11.012.

(58) Mertens, K.; Mees, G.; Lambert, B.; Van De Wiele, C.; Goethals, I. *In Vitro* 2-Deoxy-2-[^{18}F]Fluoro-D-Glucose Uptake: Practical Considerations. *Cancer Biother. Radiopharm.* **2012**, *27* (3),

183–188. https://doi.org/10.1089/cbr.2011.1125.

(59) Chouinard, J. A.; Rousseau, J. A.; Beaudoin, J.-F.; Vermette, P.; Lecomte, R. Positron Emission Tomography Detection of Human Endothelial Cell and Fibroblast Monolayers: Effect of Pretreament and Cell Density on 18FDG Uptake. *Vasc. Cell* **2012**, *4* (1), 5. https://doi.org/10.1186/2045-824X-4-5.

(60) Grkovski, M.; Goel, R.; Krebs, S.; Staton, K. D.; Harding, J. J.; Mellinghoff, I. K.; Humm, J. L.; Dunphy, M. P. S. Pharmacokinetic Assessment of ^{18}F-(2*S*,4*R*)-4-Fluoroglutamine in Patients with Cancer. *J. Nucl. Med.* **2020**, *61* (3), 357–366. https://doi.org/10.2967/jnumed.119.229740.

Appendix I

Calibration curves for determination of fluorine-18 and tritium

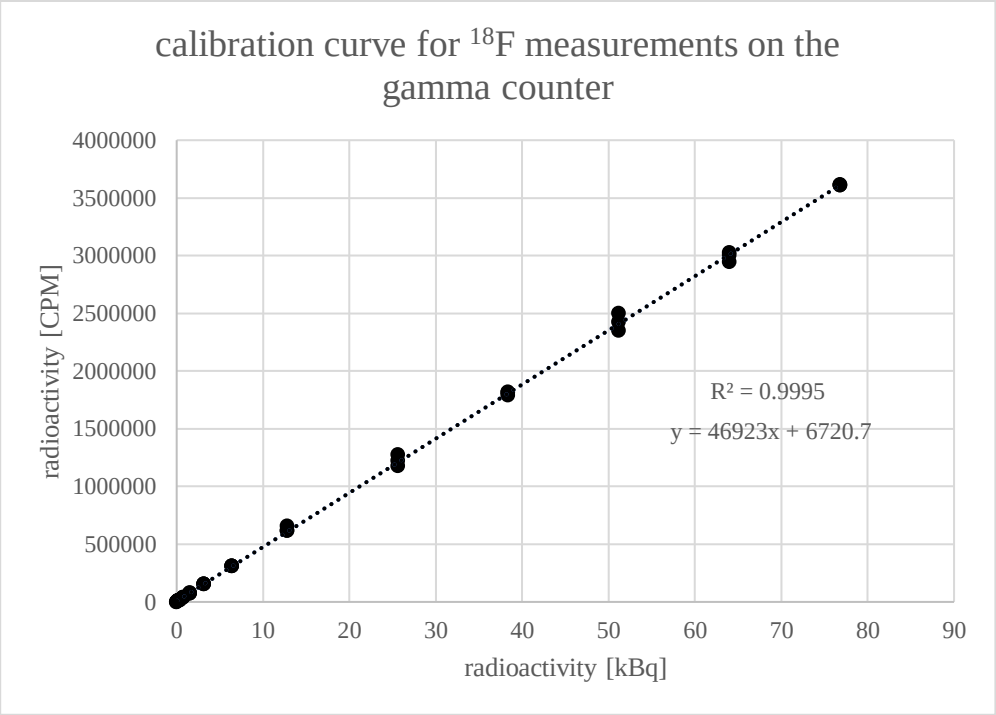

Figure 13: fluorine-18 calibration on the gamma counter

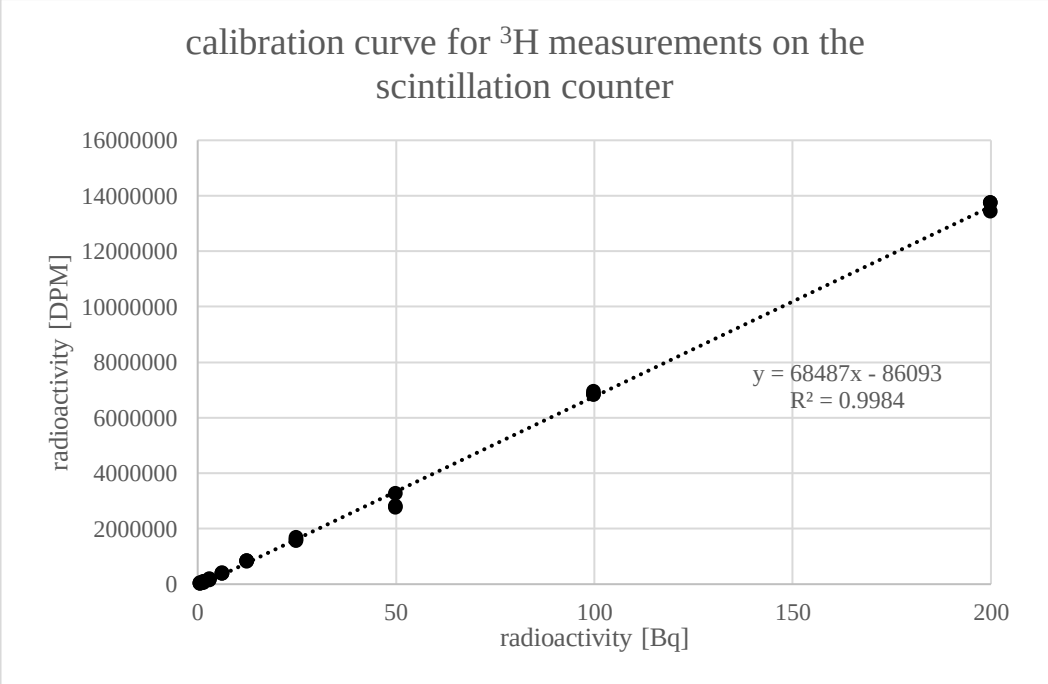

Figure 14: tritium calibration on the beta counter

Appendix II

Production of [^{18}F](2S,4R)-4-fluoroglutamine on an ELIXYS FLEX/CHEM automated synthesizer

Abbreviations:

ACN	Acetonitrile
EtOH	Ethanol
H_2O	Water
HPLC	High performance liquid chromatography
$KHCO_3$	Potassium hydrogen carbonate
MeOH	Methanol
µL	Microliter
mg	Milligram
mL	Milliliter
nm	Nanometer
PBS	Phosphate buffered saline
SPE	Solid phase extraction
TFA	Trifluoroacetic acid
TLC	Thin layer chromatography
Tosylate precursor	(2*S*,4*S*)-*tert*-butyl-2-(*tert*-butoxy-carbonylamino)-5-oxo-4-(tosyloxy)-5-(2,4,6-trimethoxybenzylamino)-pentanoate

A. General preparation:

1. Turn on argon and compressed air on control panel and hot cell.
2. Turn on general power switch below the hot cell.
3. Start ELIXYS tablet and program.
4. Purge **HPLC** system with starting solvent composition (depending on purification method), then test constant pressure on column.

   Purification option 1: **Column**: SUPERCOSIL™ LC-ABZ+ 250 x 10 µm, 5 µm. **Mobile phase**: 20-90 % ACN/water, 30 min gradient. **Flow rate**: 5 mL/min.
   Purification option 2: **Column**: Gemini® 5 µm C18 110 A 250 x 10 mm. **Mobile phase**: MeOH/water (8:2) + 0.1 % formic acid, isocratic. **Flow rate:** 5 mL/min.
   Purification option 3: purification via SPE only, without HPLC. Instead of 1 SPE cartridge, 4 are prepared and connected (see 3rd point of module preparation section). Reaction mixture containing intermediate can be transferred into dilution reservoir (prefilled with 60 mL of water) via HPLC position without a column.

5. Run PURE/FORM automated cleaning protocols for purification and formulation unit. During these, continue with further preparation.
6. Bring aliquot of 5 mg of tosylate precursor to room temperature, keep dry and dark.

B. Module preparation:

1. Prepare cassettes:

1.1 Connect red lines of each cassette with its own.
1.2 Check length of transfer line with reactor.
1.3 Check that stop-cocks at the bottom of the cassettes are in the right positions.
1.4 Fill all reactant and cleaning vials except for the precursor.

Synthesis vials:

⇒ 0.18 mL $KHCO_3$ (8 mg/mL) + 1 mL 18-crown-6 in methanol (8 mg/mL)

⇒ 2x 1 mL ACN

⇒ 1 mL TFA + 10 µL anisole

⇒ 1 mL EtOH

⇒ 1 mL PBS (pH=7.4)

⇒ 2 mL PBS (pH=7.4)

Cleaning vials:

⇒ 5x 2 mL acetone

⇒ 5x 1 mL water

⇒ 5x empty

1.5 Place vials into cassettes upside down, according to positions in schemes in the sequences:

Vial Position	Cassette 1	Cassette 2
1	$KHCO_3$ (8 mg/mL) (0.18 mL) + 18-crown-6 in MeOH (8 mg/mL) (1 mL)	TFA (1 mL) + anisole (10 µL)
2	ACN (1 mL)	EtOH (1 mL)
3	ACN (1 mL)	PBS (1 mL)
4	precursor in ACN (0.6 mL)	empty
5	/	empty
6	water (1 mL)	acetone (2 mL)
7	water (1 mL)	acetone (2 mL)
8	water (1 mL)	empty
9	acetone (2 mL)	empty
10	acetone (2 mL)	water (1 mL)
11	acetone (2 mL)	water (1 mL)
12	empty	PBS (2 mL)

1.6 Mount cassettes with vials onto ELIXYS and lock with red knobs.

1.7 Insert Chromafix® PS-HCO_3^- cartridge between blue tubes in cassette 1 and clasp into fixture on module.

2. Place two clean reactors with magnetic stir bars into the module.
3. Condition an Oasis® HLB light cartridge with 5 mL EtOH, 10 mL air and 10 mL water, connect in-between corresponding lines on PURE/FORM and clasp into fixture.
4. Connect waste 1 line with $[^{18}O]H_2O$ waste.
5. Connect green line of cassette 1 with PURE/FORM input line (valve 1).
6. Connect final product output line of PURE/FORM with one black line of cassette 2.
7. Put not needed lines into waste flask.
8. Check if PURE/FORM waste is full.
9. Fill “rinse” Falcon™ tube with 6 mL of water and make sure the line reaches the bottom of the tube.
10. Fill “elute” Falcon™ tube with a minimum of 3 mL of EtOH and make sure the line reaches the bottom of the tube.
11. Fill dilution reservoir with 18 mL of water.
12. Connect yellow line of cassette 1 with a yellow needle.
13. Connect argon line with a red needle.
14. Prepare product vial with a yellow sterile filter on a red needle and connect to green line of cassette 2.
15. Add a red needle with small white sterile filter to product vial for ventilation.
16. Fill cold trap with EtOH and dry ice.
17. Obtain fluorine-18 at cyclotron.
18. Connect activity line of cassette 1 and argon line with activity vial. Make sure yellow needle of activity line reaches the bottom of the activity vial.
19. Dissolve precursor in 0.6 mL ACN, transfer to a vial and add to cassette.
20. Close hot cell and start synthesis.

C. During synthesis:

⇒ Visually check trapping of activity on Chromafix® PS-HCO_3^- cartridge.

⇒ Observe relative activity changes in reactors and on cartridges.

⇒ If possible, check reactor cameras for successful transfer and drying steps, or select "override" until complete.

⇒ During purification collect fraction of radiolabelled intermediate (eluting after ~22 min when using purification option 1, after ~6 min using option 2) in dilution reservoir by selecting "product" in purification menu.

D. After synthesis:

1. Fill external cleaning vial with 1 mL of water and connect activity line and gas line.

2. Start cassette cleaning protocol and select "continue" at first prompt.

3. Add 1 mL of acetone to same cleaning vial at corresponding prompt and select "continue".

4. Cleaning continues automatically up to the last step.

5. At last prompt, use a syringe to push 1 mL of water, then 1 mL of acetone through black line of cassette 2, which was used for transfer from PURE/FORM.

6. Use HPLC menu to flush HPLC system with pure MeOH over a HPLC position without a column.

E. Tracer-specific quality control:

⇒ Radiochemical conversion to intermediate: **column**: Gemini® 5 µm C18 110 Å LC 250 x 4.6 mm. **Mobile phase**: methanol/water (8:2) mixture + 0.1 % formic acid. **Flow rate**: 1 mL/min flow rate

⇒ Residual anisole in product: see method above, UV measurement at 254 nm.

⇒ Radiochemical purity of product: see method above.

⇒ Stereochemical purity of product: co-injecting with non-radioactive standard 4-FGln. **Column**: Chirex® 3126 (D)-penicillamine 150 x 4.6 mm. Mobile phase: 1mM $CuSO_4$. **Flow rate:** 1 mL/min. UV measurement at 254 nm.

⇒ Free fluoride: TLC **stationary phase:** silica. **Mobile phase:** 2-propanol/acetic acid/water (3:1:1)